# Evidence for short scale stress field variations within intraplate central-western France

Y. Mazabraud, N. Béthoux, J. Guilbert, O Bellier

*Geophys. J. Int.* (2005) **160,** 161–178 doi: 10.1111/j.1365-246X.2004.02430.x

# Evidence for short-scale stress field variations within intraplate central-western France

Yves Mazabraud,[1] Nicole Béthoux,[1] Jocelyn Guilbert[2] and Olivier Bellier[3]

[1] *Géosciences Azur, UNSA,* BP48, *Villefranche sur Mer* 06235, *France. E-mails: mazab@obs-vlfr.fr (ym); nbethoux@obs-vlfr.fr (NB)*
[2] *LGS/CEA,* BP 12, *Bruyères le Chatel* 91680, *France. E-mail: jocelyn.guilbert@cea.fr*
[3] *CEREGE, Universite Aix- Marseille* 3, BP 80, *Aix-en-Provence* 13545, *France. E-mail: bellier@cerege.fr*

Accepted 2004 July 23. Received 2004 June 11; in original form 2004 March 16

## SUMMARY

Refinement of the seismicity distribution (4574 events) in western and central France, has been done by synthesis of seismological bulletins. Earthquakes have then been relocated by joint hypocentre and velocity structure inversion. The new hypocentre distribution indicates that the seismicity of those regions is much less diffuse than previously thought, mainly with regard to the depth distribution. The hypocentre improvement allows us to compute 44 new focal mechanisms and to revise bibliographic focal mechanism solutions. Then, the regional stress field was determined from 119 available focal mechanisms. It is characterized by a regionally significant strike-slip regime with NW-trending $\sigma_1$. However, the refinement in location and increasing available focal mechanism solutions allow us to show that this strike-slip regime is overprinted by local extensional perturbations in three distinct areas. In the Massif Central, the Sillon Houiller, a ancient vertical shear zone, appears to be acting as a passive boundary between a western unit and an eastern unit that is uplifted by the ascension of a hot mantle plume at the base of the lithosphere. Extension is unexpectedly observed in the southern Armorican Massif (SAM), as well as in northwestern Massif Central. One can observe a good relation between the observed perturbed zones and lateral variation of Pn anisotropy in the mantle. This correlation and the scale of these areas are arguments in favour of a lithospheric process as the origin for the stress characteristics. We believe these extensional perturbations could be related to the anticlockwise rotation of the Iberian microplate and/or incipient subduction in the Bay of Biscay.

**Key words:** focal mechanisms, France, intraplate stress field, relocation of earthquakes, seismotectonics.



## 1 INTRODUCTION

Western Europe is usually recognized as a stable intraplate region characterized by a low strain rate resulting from far field stress, originated by Europe–Africa convergence and by ridge push from the Mid-Atlantic ridge (Grünthal & Stromeyer 1992; Müller *et al.* 1992; Gölke & Coblentz 1996). However, earthquakes sometimes occur in this region, outside the recognized seismogenic zones, that include the European Cenozoic rift system (Rhêne valley, Limagne graben, Rhine graben. . .) or orogenic regions as the Alps and the Pyrenees (Fig. 1). Recent intraplate earthquakes include a $M_L$ = 5.1 event, which occurred on 1990 April 2, on the English–Welsh border (Ritchie *et al.* 1991), and three events in western France: a 1972 September 7 event in Oleron (magnitude $M_L = 5.2$), a 2001 June 8 event in Vendée (magnitude $M_L = 5.1$) and finally an event on 2002 September 30, located in SAM, of magnitude $M_L = 5.7$. To understand the occurrence of these earthquakes, it is necessary to have an accurate image of the regional microseismicity as well as constraints on the regional stress regime. The focus of the current study is twofold: (i) to improve the resolution and to upgrade the image of the seismicity in central and western France (Fig. 1); (ii) to determine the stress field throughout the study area.

Because this part of France is characterized by low and diffuse seismicity, seismotectonic studies are rather scarce (Nicolas *et al.* 1990; Delouis *et al.* 1993; Amorese *et al.* 2000). Using a seismicity catalogue that we built including arrival times from 1962 to 2002, we refined the location of the events that occurred in the Massif Central, Charente region and Armorican Massif (Fig. 2). Thanks to the computation of regional velocity models, we mainly improved the determination of the focal depths.

It is well known that fault plane solutions of local earthquakes based on *P*-wave first motions strongly depend on correct identification of wave arrivals in the seismogram and on reliable estimates of the take-off angle of the rays at the source. Therefore, revised

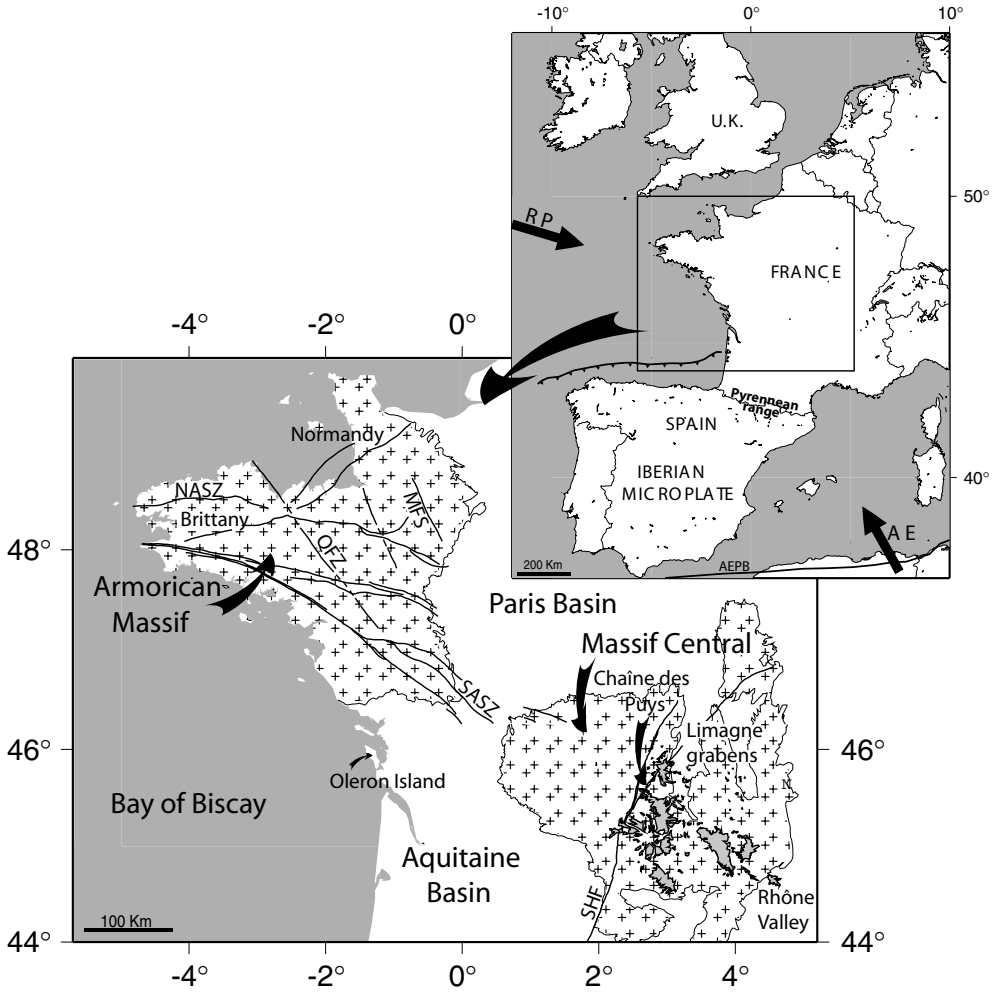


**Figure 1.** Geological setting of the study area (rectangle). Grey shaded areas in the Massif Central correspond to Cenozoic and Quaternary volcanoes. SHF: Sillon Houiller fault, SASZ: South Armorican shear zone, NASZ: North Armorican shear zone, QFZ: Quessoy fault zone, MFS: Mayenne fault system. AE: direction of the Africa–Europe convergence, RP: direction of the Mid-Atlantic ridge push, AEPB: Africa–Europe Plate boundary.

locations helped us to constrain better the computation of 44 new focal mechanisms and to revise some bibliographic focal mechanism solutions. The synthesis of these solutions and previously published mechanisms, allowed us to define the stress field, by inversion of focal mechanism solutions, using the method of Carey-Gailhardis & Mercier (1987, 1992). We observed a regionally significant strike-slip regime with a NW-trending $\sigma_1$, overprinted by three local extensional perturbations. In this paper, we do not discuss the detailed interpretation of the seismological patterns, but we focus our study on the determination of the regional stress field. A reference map for the stress determination of western Europe was published by Müller *et al.* in 1992. On the basis of this data set, Müller *et al.* (1997) interpreted the existence of perturbation zones as the coexistence of different crustal blocks with distinct stress regimes. However, the region we study was poorly constrained. Consequently, our work brings new data, allows us to refine the image of the perturbed regions and to discuss the hypothesis of crustal blocks proposed by Müller *et al.*.

## 2 GEOLOGICAL SETTING

West-central France is a slowly deforming intraplate region. It is composed of two Hercynian massifs, the Massif Central and the Armorican Massif, separated by two great Mesozoic sedimentary basins, the Paris basin and the Aquitaine basin (Fig. 1). In the east, the Alps are separated from the Massif Central by the Rhêne valley, which is part of the European Cenozoic rift system (as well as the Limagne graben). In the west, are the passive margins of the Atlantic ocean and the Bay of Biscay. The opening of the Bay of Biscay, beginning 114 Ma (Montardet *et al.* 1979; Olivet 1996), and now its closure by early stage subduction (Ayarza *et al.* 2004), together with the Pyrennean range separates the Iberian microplate from the European Plate. Synchronous to the development of the Cenozoic Limagne graben, volcanism occurred in the Massif Central but no volcanism has occurred west of the Sillon Houiller fault (SHF). This area is still potentially active as the youngest volcanoes are 7000 yr old (Nehlig *et al.* 2001). Several studies show a hot thermal anomaly beneath the Massif Central (Froidevaux *et al.* 1974; Vasseur 1982; Granet *et al.* 1995a; Sobolev *et al.* 1996), associated with a mantle plume, whose origin is still debated (Merle & Michon 2001). The major faults of the Massif Central and the Armorican Massif are the SHF and the South Armorican shear zone (SASZ). The French Hercynian massifs are mainly composed of granitic and metamorphic rocks. The Paris and Aquitaine basins are composed of quasi-undeformed, unmetamorphosed sedimentary rocks. They have a maximum thickness of 3000 and 10 000 m

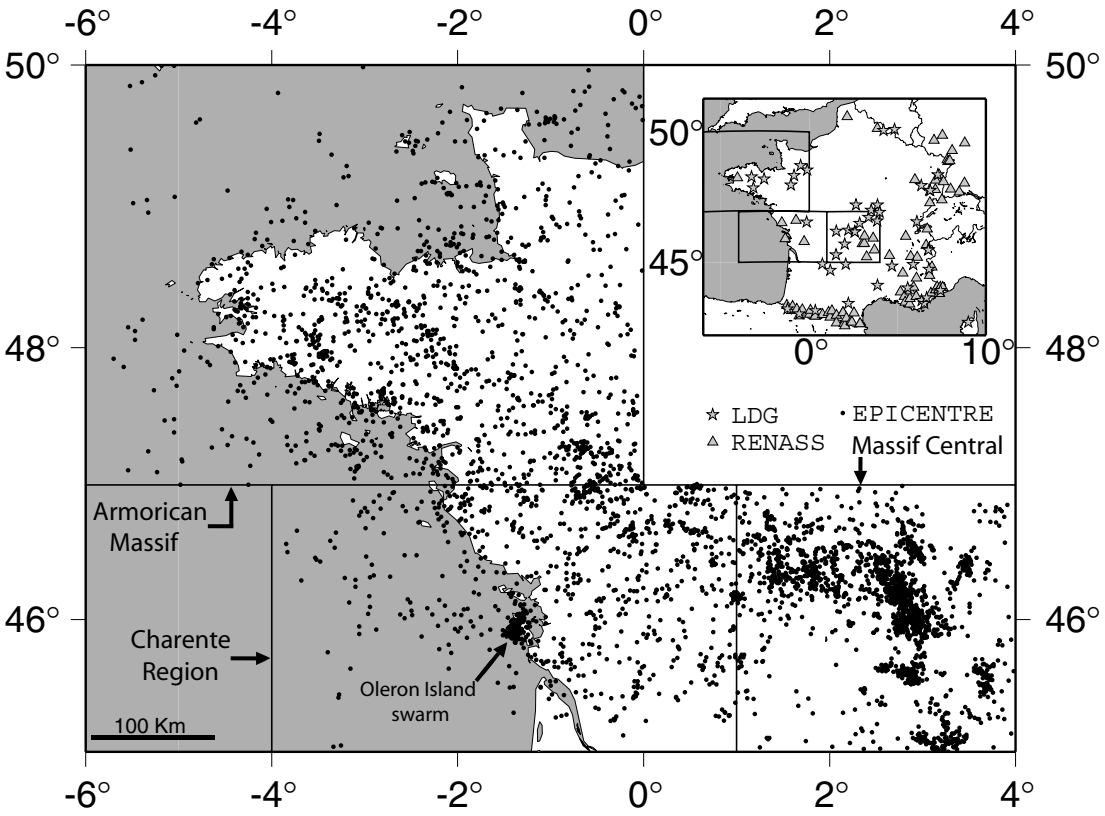


**Figure 2.** All epicentres (black dots) of the study area. Rectangles enclose the Massif Central, the Charente region and the Armorican Massif subregions. Grey stars are the seismic stations of the LDG network and grey triangles are the stations of the ReNaSS network.

respectively and their basement is of the same nature as the surrounding massifs.

## 3 SEISMICITY DISTRIBUTION

### 3.1 Location procedure

#### *3.1.1 Building of the catalogue*

4574 events have been recorded from 1962 January 1 to 2002 January 1 in the study area, by the *Laboratoire de Détection Géophysique* (LDG) network and, since 1980, by the French National Seismic Network (Réseau National de Surveillance Sismique, ReNaSS). The catalogues of these two institutes, along with some data of the European–Mediterranean Seismological Centre (CSEM) have been combined month by month, from 1962 January to 2001 December. The data from CSEM include data from the British, Irish, Spanish, Portuguese, Belgian and Swiss networks.

As a first step, we located all the events using a code written at LDG (hereafter called FUSION), which considers both *Pn* and *Pg* phases (and corresponding *Sn* and *Sg* phases). The LDG was created in 1960 and, because at this time there were few seismological stations available, the seismologists of this institute identified both *Pn* and *Pg* phases (and associated *Sn* and *Sg* phases). This procedure allows the number of arrival times to be doubled and an additional constraint to be brought to the event depth determination through the (*Pn–Pg*) arrival times difference. This picking procedure is still used by LDG, despite the densification of the network, whereas conventional routines such as HYPO71 (Lee & Lahr 1975) only takes into account one *P*-wave first arrival time and one *S*-wave arrival time. The FUSION algorithm is classically based on the Geiger method (Geiger 1910). Only origin time, epicentral latitude and longitude are inverted from the matrix of arrival times. The depth is used as a parameter in the traveltime computation and the final depth value (tested at a step size of 1 km) is the one that provides the best statistical results (in term of the rms of arrival times and axes of the true confidence ellipse). The locations are performed with all the available stations (Fig. 2) and the LDG 1-D crustal velocity model (M0 in Table 1a), a simple model appropriate for wide areas across France.

We compared this location procedure with the standard HYPO71 solutions. As microseisms are only detected by the closest stations, only the direct *Pg* and *Sg* are available so the results are identical. For larger magnitude events, recorded at long-range distance, we verified that FUSION brings generally more stability than HYPO1D in the hypocentral determination. This is particularly true for events of western Britanny, which are located with sparse regional distance stations. Corresponding seismograms depict energetic *Pg* and *Sg* waves, whereas *Pn* and *Sn* are very attenuated along these particular ray paths. In this case, automated picking, which works well for the first *P* arrival, would deal with misidentification and erroneous locations.

On Fig. 2, the seismicity of the northern Massif Central, the Armorican Massif and the Charente region is displayed. The seismological stations correspond to triangles (ReNaSS) or stars (LDG), whereas black dots are the epicentre locations. So, the first step of the work presented here was the building of a complete and reliable catalogue of uniformly located hypocentres for the whole studied region, with local magnitude from 2.0 to 5.7.

**Table 1a.** M0 model: starting model derived from the very simple model used in FUSION code. WMC0: the *a priori* model chosen as a starting model. It is deduced from Zeyen *et al.* (1997), for crustal velocities and from Juhenderc & Granet (1999) for the *Pn* velocity. WMC1: the final model deduced from VELEST, with WMCO model, as the starting model. WMC2: the final model generated by the convergence of the inversion of 50 random initial models.

| M0 | | WMC0 | | WMC1 | | WMC2 | |
|---|---|---|---|---|---|---|---|
| Depth | *Vp* | Depth | *Vp* | Depth | *Vp* | Depth | *Vp* |
| −2.5 | 3.5 | −2.5 | 5.5 | −2.5 | 3.5 | −2.5 | 3.5 |
| 0 | 3.5 | 0 | 5.95 | 0 | 5.4 | 0 | 5.98 |
| 1 | 6.03 | 1 | 5.95 | 1 | 5.9 | 1 | 5.9 |
| 4 | 6.03 | 4 | 5.95 | 4 | 6.0 | 4 | 6.0 |
| 8 | 6.03 | 8 | 6.05 | 8 | 6.05 | 8 | 6.02 |
| 12 | 6.03 | 12 | 6.10 | 12 | 6.15 | 12 | 6.20 |
| 15 | 6.03 | 15 | 6.30 | 15 | 6.20 | 15 | 6.20 |
| 20 | 6.03 | 20 | 6.40 | 20 | 6.35 | 20 | 6.20 |
| 26 | 8.10 | 25 | 6.60 | 25 | 6.35 | 25 | 6.38 |
| 30 | 8.10 | 30 | 8.00 | 30 | 8.16 | 30 | 8.15 |

**Table 1b.** The same for CHP and LIM velocity models.

| CHP0 | | CHP1 | | CHP2 | | LIM0 | | LIM1 | | LIM2 | |
|---|---|---|---|---|---|---|---|---|---|---|---|
| Depth | *Vp* | Depth | *Vp* | Depth | *Vp* | Depth | *Vp* | Depth | *Vp* | Depth | *Vp* |
| −2.5 | 3.5 | −2.5 | 3.5 | −2.5 | 3.5 | −2.5 | 3.5 | −2.5 | 3.08 | −2.5 | 3.62 |
| 0 | 5.0 | 0 | 5.07 | 0 | 5.45 | 0 | 4.06 | 0 | 3.92 | 0 | 5.14 |
| 2 | 5.5 | 2 | 5.72 | 2 | 5.80 | 2 | 5.57 | 2 | 5.91 | 2 | 5.92 |
| 4 | 5.6 | 4 | 5.87 | 4 | 6.05 | 4 | 5.70 | 4 | 6.00 | 4 | 5.92 |
| 8 | 5.9 | 8 | 6.06 | 8 | 6.15 | 8 | 6.0 | 8 | 6.02 | 8 | 6.05 |
| 12 | 6.1 | 12 | 6.10 | 12 | 6.20 | 12 | 6.10 | 12 | 6.43 | 10 | 6.22 |
| 15 | 6.3 | 15 | 6.10 | 15 | 6.43 | 15 | 6.10 | 15 | 6.50 | 15 | 6.62 |
| 20 | 6.4 | 20 | 6.54 | 20 | 6.71 | 20 | 6.35 | 20 | 5.50 | 20 | 6.62 |
| 25 | 6.5 | 25 | 7.09 | 25 | 6.97 | 25 | 8.10 | 25 | 7.30 | 27 | 7.35 |
| 30 | 7.7 | 30 | 7.22 | 30 | 7.20 | 30 | 8.10 | 30 | 7.80 | 30 | 8.00 |

**Table 1c.** The same for CHAR velocity models.

| CHAR0 | | CHAR1 | | CHAR2 | |
|---|---|---|---|---|---|
| Depth | *Vp* | Depth | *Vp* | Depth | *Vp* |
| −2.5 | 3.03 | −2.5 | 3.04 | −2.5 | 3.03 |
| 0 | 3.50 | 0 | 4.04 | 0 | 4.70 |
| 1 | 5.50 | 1 | 5.83 | 1 | 5.88 |
| 5 | 6.03 | 5 | 5.83 | 5 | 5.97 |
| 10 | 6.03 | 10 | 6.11 | 10 | 5.97 |
| 15 | 6.03 | 15 | 6.11 | 15 | 6.20 |
| 20 | 6.03 | 20 | 6.66 | 20 | 6.50 |
| 25 | 6.03 | 25 | 6.90 | 25 | 6.50 |
| 30 | 8.10 | 30 | 8.00 | 30 | 8.00 |

### *3.1.2 Relocation of the events*

Our second aim was to improve the hypocentral location of the events using a more realistic velocity model. We did this by dividing the area into subregions in order to take into account their geological differences and the geometry of the network.

In some areas, where the number of events and the distribution of seismological stations allowed, we relocate the seismicity using a technique of simultaneous determination of the velocity model and the earthquake hypocentres (Ellsworth 1977). The main task of this method is to minimize the errors resulting from both the model parameters and arrival times. We relocated these regional groups of events through the application of the program VELEST written by Kissling *et al.* (1984), which allows us to invert the minimum 1-D model with station corrections and hypocentre parameters, which minimizes the rms residual of the full data set.

For each area, we selected the best events, that is to say those with the highest quality arrivals (axes of the confidence ellipse smaller than 10 km, as computed by FUSION; with at least seven stations) and that cover the entire area under consideration.

VELEST uses only one *P* and one *S* arrival time and, with the intention of this being a regional-scale study, we only used stations at less than 200 km epicentral distance. We used *Pn* and *Sn* for the regional-distance stations and kept *Pg* and *Sg* phases for the closest stations. Therefore, we favoured the use of *Pg* and *Sg* phases but kept enough *Pn* and *Sn* to determine Moho depth and velocity.

The determination of this minimum 1-D model is a trial and error process, which starts with an *a priori* velocity model. Our initial models (that we call model 0, in the following discussion) were based preferably on refraction seismic profiles, as recommended by Kissling *et al.* (1994).

We first computed final models (the so-called model 1), by conducting a series of successive 1-D inversions and relocations, in order to minimize the final global variance of our set of location data.

In a second step, we conducted a grid search of the *a priori* 1-D model, by introducing random changes of layer velocities ($\leq 1$ km $s^{-1}$) in the updated *a priori* model (model 1). A plot of the velocity models resulting from the inversions allows us to show that these models converge towards an average model (model 2) and provides knowledge of the variations of resolving power with depth. The aim of this procedure is to verify the stability of the results considering both the final minimum 1-D model and location parameters.

### *3.1.3 The depth of the events*

Some general comments about depths can be made. In the Massif Central and Charente regions, most earthquakes are shallow (depth

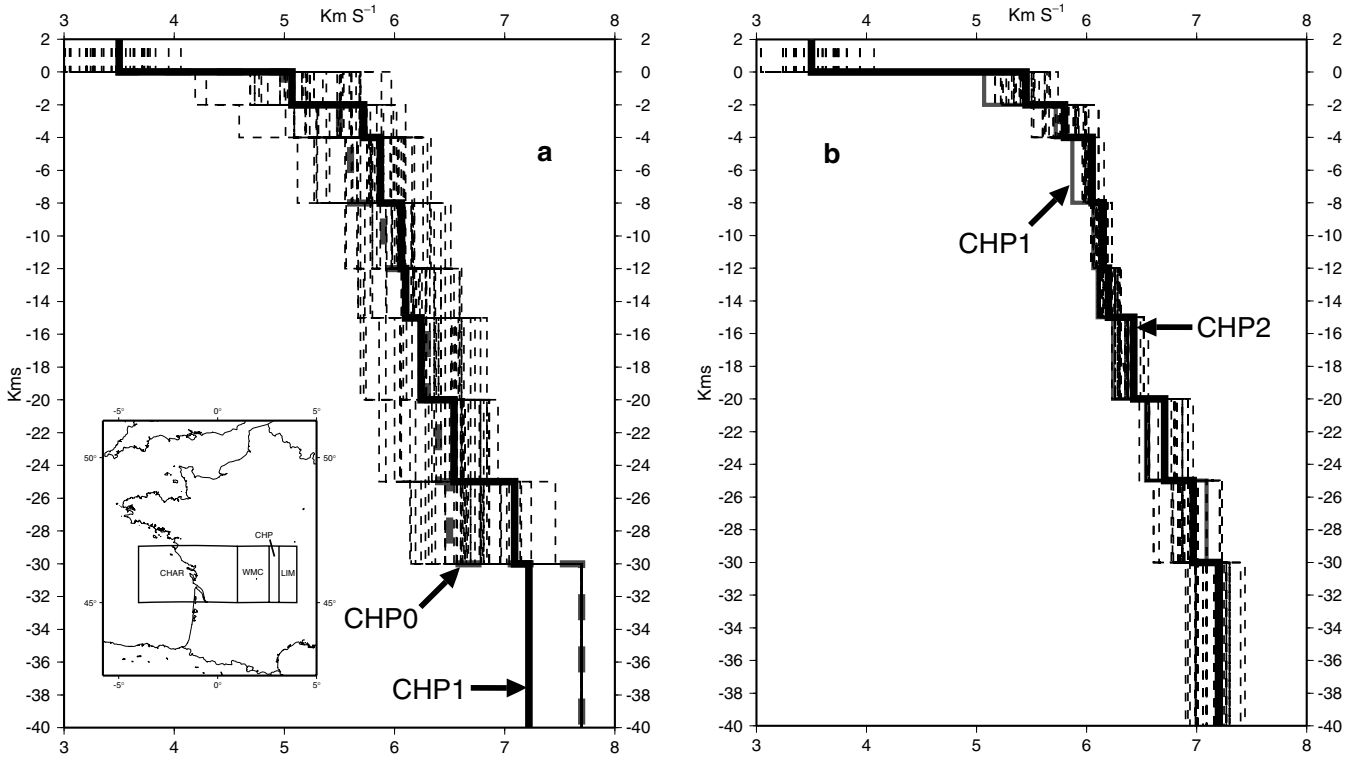


**Figure 3.** Example of inversions for a 1-D model for the CHP area. (a) The initial model CHP0 is deduced from seismic results shown by bold, grey dashed line, the inverted model CHP1 is the bold black line and the initial random models generated from CHP1 model are thin dashed lines. (b) At the end of the inversion process, the resulting models are the thin dashed lines. The convergence of the velocities around a single model CHP2 is shown by the bold line and consequently chosen as the best minimum 1-D model. The grey line corresponds to CHP1 (the resulting model after the first iteration).

$\leq$ 8 km), nevertheless, they are all located in the basement Hercynian rocks. The seismogenic crust has a thickness of 11 $\pm$ 1 km (Fig. 3). No discrepancy is observed between the shallowest and the deepest focal mechanisms. Moreover, the small topographic variations of this area cannot be invoked for any stress variation with depth. Thus, we consider that these earthquakes testify to the style of faulting in this area. Indeed, these focal solutions are consistent with the over-coring data from Cornet & Burlet (1992) that show a rotation of $\sigma_{\mathrm{Hmax}}$ towards the E–W in the eastern Massif Central (EMC). Reliability of hypocentral determination in the Armorican Massif is not good enough to allow detailed interpretation of the revised depths of the earthquakes. Nevertheless, considering only the strongest and best located events, the seismogenic crust seems to be 12 $\pm$ 1 km thick.

### *3.1.4 The Massif Central*

In the Quaternary volcanic Massif Central, 2292 events are clustered in tectonically active areas: along the volcanic area, near the Limagne graben and where the SASZ ends. So, we divided this area, into three subregions (Fig. 3). They are the so-called western Massif Central (WMC), the Chain of Puys (CHP) and the Limagne region (LIM). First, we chose the three models WMC0, CHP0 and LIM0 to be applied in the three studied areas, on the basis of the seismic refraction results from Zeyen *et al.* (1997). These models are given in Tables 1(a) and (b). Then, we followed the procedure described above : first, we computed three models WMC1, CHP1 and LIM1 (Tables 1a and b). We conducted a grid search of the *a priori* 1-D model, by introducing random changes of layer velocities ($\leq$ 1 km s$^{-1}$), in the WMC1, CHP1 and LIM1 models. Fig. 3(a) displays an example of random initial models, for the CHP area, around the inverted model CHP1. Fig. 3(b) shows the convergence of velocities around a single model, CHP2, close to the model CHP1. Nevertheless, the 1-D model is less resolved at depth >20 km than for the shallower layers. This model was chosen as a new starting model in a new inversion sequence to obtain the final locations. Table 1 presents the starting and final velocity models obtained by inversion, then the final minimum 1-D model we determined for each area.

Strictly speaking, the minimum 1-D model deduced from this study does not represent a true geophysical image of the studied areas. It consists of an average velocity model in the medium crossed by the rays from the hypocentral zone to the stations, which is deduced from a trial and error approach using an earthquake and station data set. However, in this study, we selected only stations that are close to the epicentre area. Consequently, the best minimum 1-D model obtained can be evaluated in terms of the regional structure. We can observe that all the inverted CHP and LIM models tend to have a low-velocity layer at the bottom of the model (Fig. 2), still lower than the anomalous low velocity obtained by seismic refraction for the upper mantle (Table 1b). Controversially, models computed for the WMC area are characterized by rather homogeneous and high crustal velocities. Note that, the final minimum 1-D models are very close to the results obtained by Juhenderc & Granet (1999) using anisotropic tomographic modelling beneath France. Their tomographic image of *Pn* velocity perturbation clearly shows high *Pn* velocities, up to 8.15 km s$^{-1}$ in the west of Massif Central, whereas, crossing the SHF (Fig. 1), the *Pn* velocity decreases dramatically down to 7.66 km s$^{-1}$. This low-velocity region coincides with the main volcanic areas and these low velocities are associated

**Table 2.** Data and model variances for the 1-D models. Initial data variances were measured after the first relocation by VELEST using the starting model. The final variance are results from six iterations of the direct inversion with the final velocity model.

| | Number of located events | Initial variance ($s^2$) | Final variance ($s^2$) |
|---|---|---|---|
| MCO | 454 | 0.59 | 0.37 |
| CHP | 455 | 1.23 | 0.43 |
| LIM | 304 | 1.21 | 0.74 |
| CHAR | 541 | 1.98 | 0.66 |

with the high temperature related to the Neogene volcanic activity (Sobolev *et al.* 1997). We also find low *Pn* velocity beneath the Limagne graben, as already obtained by Perrier & Ruegg (1973) from refraction results.

Table 2 shows the improvement in the variance obtained during the procedure. In Fig. 4 we present the comparison between 1242 hypocentre locations performed in the first part by FUSION and in the second part by VELEST. The epicentral parameters are similar and preliminary ill-located events are rather scarce. Nevertheless, the relocated events tend to be more clustered and orientated closer to the direction of geological structures. However, the projection of hypocentres along two vertical cross-sections, allows us to show the main differences between the two series of results. The focal depths are dramatically shifted. The seismogenic zone is limited to 10 km depth and the hypocentres are more clustered, as shown on the two vertical cross-sections. Furthermore, we verified that the change of velocity models (as explained in Section 3.1.2) did not imply dramatic change of focal depth. From comparison between the different locations obtained with VELEST, we deduced the maximum uncertainties in depth are ±1 km.

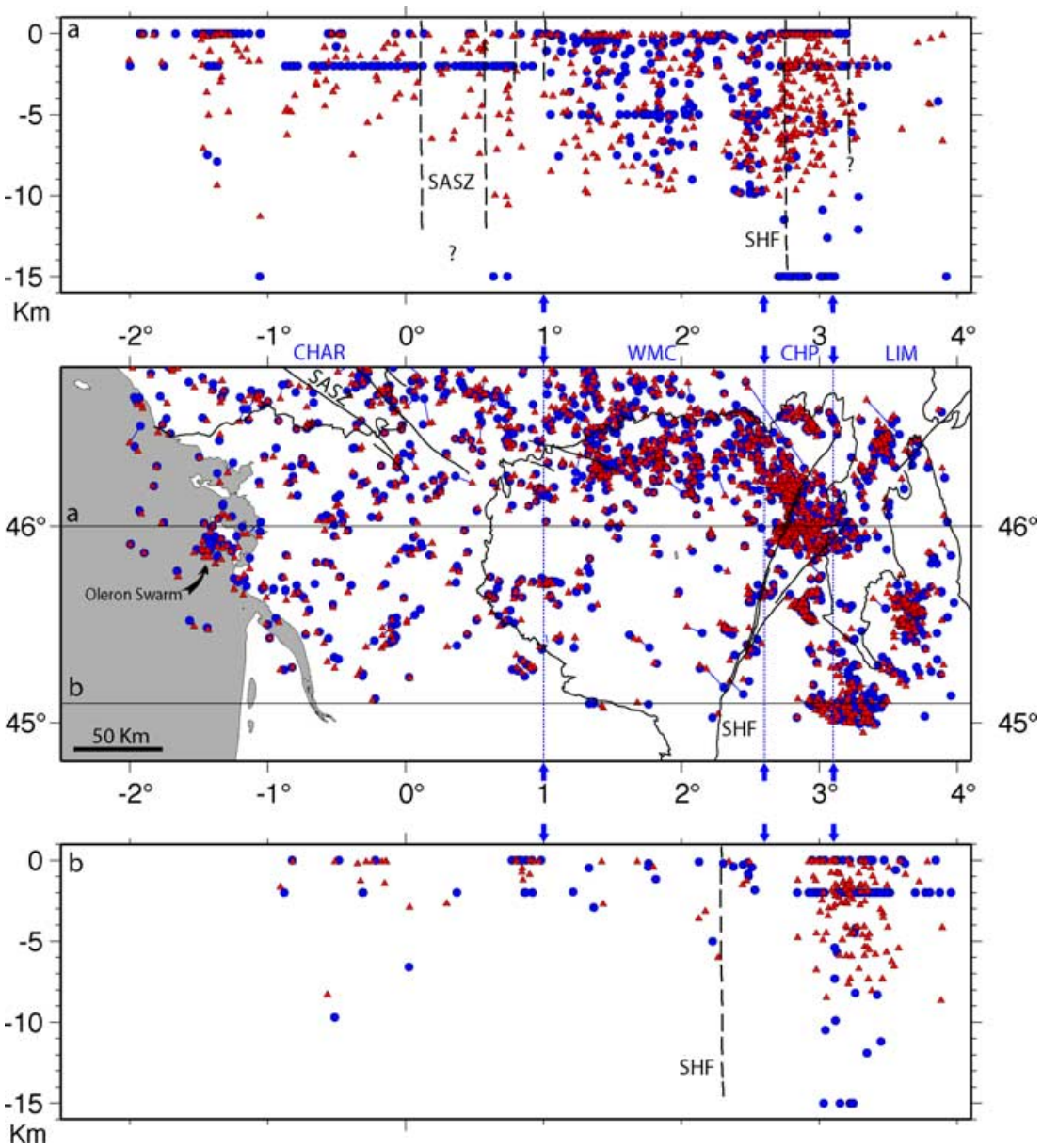


**Figure 4.** Comparison of epicentres and hypocentres of the Charente region and Massif Central located with the M0 model (Table 1a), shown as circles, and relocated by the joint velocity–velocity model inversion (black triangles). Hypocentres are displayed on two east–west cross-sections, at 45.1 and 46.0 latitude north. Hypocentres plotted lie within 15 km of the cross-section lines. SASZ: South Armorican shear zone, SHF: Sillon Houiller fault.

A detailed interpretation of the seismological patterns is beyond the scope of this publication and will be the subject of a separate article (Mazabraud *et al.* 2005).

Therefore, the VELEST code allows us to find realistic crustal models that can be now used for the location of the local seismicity. They allow us to constrain the focal depth better than the 1-D average velocity model of Table 1(a) (M0).

#### *3.1.5 The Charente region*

981 events are recorded in the region. The 1972 Oleron Island swarm, in the centre of the area, clearly contrasts with the surrounding more diffuse seismicity (Figs 2 and 4).

Without available refraction data, we began with a simple velocity model derived from the one already used in the location process with FUSION (M0, Table 1a), but with more layers, in order to obtain a better inverted minimum 1-D model that fits the data set [model CHAR1; then CHAR2 (Table 1c) obtained with the procedure previously described]. The azimuthal coverage of the stations is limited to 180°–200°. So, this velocity model has no geological significance and the procedure only allows us to compute station corrections and to obtain joint hypocentre locations. Once again, the variance is improved (Table 2). The main change in hypocentres (Fig. 4) still relates to the depth of the events, which consistently deepens from west to east.

#### *3.1.6 The Armorican Massif*

The peninsular shape of the Massif provides poor azimuthal coverage by the networks and most of the events were only recorded by regional-distance stations. Therefore, the relocation methodology could not be applied for this westernmost region. We only benefit from the FUSION location catalogue, which provides rather numerous seismic events (1301 events) for this region. The dispersion of the seismicity (Fig. 2) is partly the result of the poor azimuthal coverage. Moreover, the focal depths are usually not constrained. Nevertheless, the largest magnitude events ($M_L > 4.0$) are recorded by British and Spanish stations and produce more reliable locations. Since 1996, installation of stations in Brittany (Fig. 1) allows a significant improvement in location.

## 4 FOCAL MECHANISMS

Taking into account the improvement in the epicentral coordinates, mainly in hypocentral determination and in the velocity model, we can compute more realistic take-off angles to determine new focal mechanism solutions.

### 4.1 New Earthquake fault-plane solutions

Focal mechanisms have been computed by means of the FPFIT code (Reasenberg & Oppenheimer 1985), which systematically searches the solution space for the double-couple fault plane solutions that best fit, in a least-squares sense, a given set of observed first-motion polarities. This method may determine several solutions with related uncertainties for both nodal planes. For the best-constrained mechanisms, only one solution is obtained.

In the current study, we have determined 44 new earthquake focal mechanisms. The selected solutions are reported in Table 3 and shown in Fig. 5.

### 4.2 Previously published focal mechanisms

Focal mechanisms from other events that occurred in the studied region have already been published (Delhaye 1976; Santoire 1976; Veinante-Delhaye & Santoire 1980; Nicolas *et al.* 1990). These authors used the LDG velocity model to determine the focal mechanism solutions.

We revised these solutions with the help of the new hypocentral determinations and velocity model. Some mechanisms have been computed with a majority of *Pn* polarities. In this case, the change of take-off angles is small, even with a shift of focal depth and a different velocity model. Some others, computed with many *Pg* polarities, are more sensitive to the focal depth and velocity model. All previously published focal mechanism solutions are reported in Table 4. Only eight events have clearly different solutions after revision. They are indicated by a star in Table 4 and are displayed on Fig. 5.

Dorel *et al.* (1995) and Amorese *et al.* (2000) computed focal mechanisms from dense local networks in Normandy and the EMC (Fig. 1), with realistic take-off angles. We used their solutions without revision.

### 4.3 Quality of the focal mechanism solutions

To each focal mechanism solution, a quality factor has been assigned. We took into account the error limits, as computed by FPFIT (strike and dip uncertainties: ΔSTR, ΔDIP) and solution quality through a parameter $F$, which qualifies a data misfit measure) and the magnitude of the earthquakes.

Then, following Zoback (1992), we classified the available mechanisms into four classes (A–D).

A: $M_L \geq 4$ and well-constrained solutions (ΔSTR, ΔDIP $<20°$ and $F < 0.025$).

B: $M_L \geq 4$ and less constrained or $3 \leq M_L < 4$ and well constrained.

C: $2 \leq M_L < 3$ and well constrained or $3 < M_L < 4$ and less constrained.

D: $M_L < 2$ or poorly constrained solutions.

Only one exception was made for the focal mechanism solutions that we determined with local network data that can lead to reliable solutions even for magnitudes $\leq 3$. These solutions are classified as C.

### 4.4 Results

A synthesis of the previously published and newly calculated focal mechanism solutions for the Armorican Massif is plotted in Fig. 6(a). In the south, most mechanisms are characterized by a dominant normal-slip component and a NNE-trending $T$-axis, whereas in the north, the type of mechanism is less coherent, with E-trending $T$-axis in the northwest of the massif and nearly NE-trending $T$-axis northeast of the massif. In the southeast, only two mechanisms (n°101 and n°109) do not seem consistent with the other ones. They are more likely related to the mechanisms of the northeastern Charente region and northwestern Massif Central that show nearly NW-trending $T$ axes.

Fig. 6(b) shows the new and the published focal mechanisms for the Charente region. Most solutions are compressional or strike-slip, with a NE to E trending $T$-axis. The seismic crisis of Oleron Island, that began in 1972 with a $M_L = 5.2$ event (n°82) and lasted more than 10 yr, is represented by five focal mechanisms (82, 83, 87, 88 and 91). However, they also have a normal component and n° 88 is purely extensional. Four of them are strike-slip. The $M_L = 5.2$ event (n° 37), of 2001 June 8, is located at 12 km depth, on the southeastern

**Table 3.** New focal mechanisms. The focal mechanisms are classified by date for each geographical region. The stress field zone is determined *a posteriori* by stress field inversion.

| Geographical area | Number | Stress field zone | Date (YYYY/MM/DD) | Time (UTC) (HH/MM/SS) | Long. (°) | Lat. (°) | Depth (km) | Mag (Ml) | Quality | Plane A | | | Plane B | | | *P*-axis | | *T*-axis | |
|---|---|---|---|---|---|---|---|---|---|---|---|---|---|---|---|---|---|---|---|
| | | | | | | | | | | Az | Dip | Vect. | Az | Dip | Vect. | *P* az. | *P* dip. | *T* az. | *T* dip. |
| Central Massif | | | | | | | | | | | | | | | | | | | |
| | 1 | CHAR | 1989/05/03 | 7:44:11 | 2.4589 | 46.3554 | 6.99 | 3.9 | B | 151 | 80 | −3 | 242 | 87 | −170 | 107 | 11 | 16 | 3 |
| | 2 | CHMC | 1990/07/06 | 19:00:31 | 1.3016 | 46.552 | 0.05 | 3.4 | B | 255 | 88 | −23 | 346 | 67 | −178 | 207 | 20 | 304 | 17 |
| | 3 | CHAR | 1991/05/22 | 13:41:12 | 1.8231 | 46.3667 | 0.01 | 3.7 | D | 115 | 77 | 177 | 206 | 87 | 13 | 340 | 6 | 71 | 12 |
| | 4 | CHAR | 1991/05/30 | 9:15:26 | 1.8339 | 46.3577 | 5.00 | 3.3 | B | 134 | 53 | −113 | 349 | 43 | −63 | 346 | 71 | 240 | 5 |
| | 5 | CHAR | 1991/06/09 | 0:34:04 | 1.8893 | 46.2808 | 5.00 | 3.5 | B | 112 | 81 | 177 | 202 | 87 | 9 | 337 | 6 | 67 | 6 |
| | 6 | ECM | 1991/06/27 | 4:44:12 | 2.9985 | 45.0944 | 1.87 | 3.4 | B | 120 | 60 | −41 | 233 | 55 | −143 | 85 | 49 | 177 | 2 |
| | 7 | ECM | 1991/07/28 | 1:54:25 | 3.2208 | 45.2356 | 0.18 | 3.4 | C | 241 | 76 | 141 | 342 | 52 | 18 | 296 | 15 | 195 | 37 |
| | 8 | CHMC | 1992/09/23 | 2:41:38 | 1.088 | 46.7871 | 1.46 | 3.2 | C | 30 | 34 | −160 | 283 | 79 | −58 | 226 | 46 | 348 | 27 |
| | 9 | ECM | 1993/09/02 | 3:13:46 | 2.986 | 45.0959 | 6.06 | 3.0 | B | 5 | 67 | −120 | 241 | 37 | −40 | 234 | 57 | 117 | 17 |
| | 10 | ECM | 1993/10/17 | 22:57:01 | 3.88 | 45.2492 | 1.10 | 3.6 | C | 148 | 88 | 145 | 239 | 55 | 2 | 197 | 17 | 100 | 20 |
| | 11 | CHAR | 1994/01/29 | 0:31:00 | 1.5688 | 46.6978 | 8.66 | 3.7 | B | 13 | 48 | −54 | 146 | 53 | −123 | 354 | 64 | 259 | 3 |
| | 12 | CHAR | 1994/12/18 | 2:56:01 | 1.4316 | 46.4011 | 4.70 | 3.0 | C | 139 | 85 | −77 | 250 | 14 | −159 | 63 | 48 | 217 | 39 |
| | 13 | CHAR | 1995/02/24 | 9:05:54 | 1.5624 | 46.599 | 0.91 | 3.2 | C | 21 | 85 | 20 | 289 | 70 | 175 | 153 | 12 | 247 | 19 |
| | 14 | ECM | 1995/05/11 | 23:10:07 | 3.8108 | 45.2633 | 3.32 | 3.1 | C | 121 | 86 | 138 | 215 | 48 | 5 | 177 | 27 | 68 | 33 |
| | 15 | ECM | 1995/05/14 | 6:45:59 | 3.0825 | 45.3027 | 0.63 | 3.2 | B | 11 | 87 | −9 | 101 | 81 | −177 | 326 | 2 | 56 | 2 |
| | 16 | ECM | 1995/07/30 | 10:13:21 | 3.6321 | 45.6134 | 0.44 | 3.1 | D | 211 | 66 | 119 | 338 | 37 | 43 | 281 | 16 | 162 | 59 |
| | 17 | CHAR | 1995/09/15 | 18:24:26 | 1.4997 | 46.3232 | 8.68 | 3.3 | B | 19 | 73 | 23 | 282 | 68 | 162 | 150 | 3 | 241 | 28 |
| | 18 | CHMC | 1996/06/25 | 5:10:13 | 1.0264 | 46.5184 | 3.61 | 3.4 | B | 30 | 76 | −123 | 280 | 36 | −25 | 264 | 48 | 145 | 24 |
| | 19 | CHMC | 1997/08/23 | 15:07:18 | 1.2515 | 465038 | 0.52 | 3.6 | B | 64 | 57 | 29 | 317 | 66 | 143 | 12 | 5 | 277 | 42 |
| | 20 | ECM | 1997/08/29 | 0:55:33 | 3.6343 | 45.5913 | 5.00 | 3.6 | B | 102 | 60 | −122 | 333 | 43 | −47 | 322 | 61 | 214 | 10 |
| | 21 | CHAR | 1997/11/14 | 23:52:02 | 2.1795 | 46.554 | 1.43 | 3.1 | B | 95 | 51 | −157 | 350 | 72 | −41 | 305 | 41 | 47 | 13 |
| | 22 | ECM | 1999/01/19 | 1:29:21 | 2.8067 | 45.9654 | 1.81 | 3.4 | B | 46 | 43 | 163 | 149 | 78 | 48 | 269 | 22 | 20 | 41 |
| | 23 | CHMC | 2000/05/06 | 13:33:04 | 1.4321 | 46.4934 | 5.00 | 3.3 | B | 252 | 79 | −41 | 351 | 50 | −166 | 204 | 35 | 307 | 18 |
| | 24 | ECM | 2000/07/13 | 1:50:47 | 3.0183 | 45.8877 | 9.25 | 3.3 | B | 28 | 65 | 60 | 262 | 38 | 137 | 140 | 15 | 255 | 59 |
| | 25 | ECM | 2001/05/29 | 11:10:02 | 3.5902 | 45.6212 | 7.84 | 3.1 | B | 223 | 73 | −2 | 314 | 88 | −163 | 180 | 14 | 87 | 10 |
| | 26 | ECM | 2001/11/05 | 8:53:13 | 3.7429 | 45.5787 | 5.75 | 3.4 | B | 101 | 34 | −162 | 356 | 80 | −57 | 299 | 45 | 60 | 28 |
| | 27 | CHAR | 2000/12/05 | 11:53:27 | 1.6207 | 46.3658 | 3.84 | 3.0 | C | 8 | 71 | 35 | 265 | 57 | 157 | 134 | 9 | 231 | 38 |
| Charente Region | | | | | | | | | | | | | | | | | | | |
| | 28 | CHMC | 1996/06/10 | 0:53:02 | 0.6937 | 46.9613 | 3.64 | 3.0 | C | 64 | 75 | −70 | 188 | 25 | −143 | 0 | 55 | 137 | 27 |
| | 29 | CHAR | 1996/12/01 | 11:52:46 | 0.0269 | 45.8621 | 1.62 | 3.9 | B | 39 | 56 | 43 | 281 | 56 | 137 | 160 | 0 | 250 | 53 |
| | 30 | CHAR | 1997/01/12 | 1:24:16 | −1.1405 | 46.534 | 9.89 | 4.0 | A | 17 | 42 | 48 | 247 | 60 | 121 | 315 | 10 | 207 | 62 |
| | 31 | CHAR | 1997/09/30 | 3:05:00 | 0.0327 | 46.3533 | 5.00 | 3.0 | C | 171 | 81 | −2 | 261 | 88 | −171 | 126 | 6 | 36 | 6 |
| | 32 | CHAR | 1997/11/25 | 13:20:13 | −1.3618 | 46.9255 | 5.00 | 3.0 | C | 117 | 89 | 113 | 210 | 23 | 3 | 190 | 41 | 45 | 43 |
| | 33 | CHAR | 2000/02/23 | 15:46:42 | 0.3507 | 45.4155 | 2.02 | 4.1 | A | 11 | 79 | 40 | 272 | 51 | 166 | 136 | 18 | 239 | 35 |
| | 34 | CHAR | 2000/05/02 | 6:52:10 | −1.9241 | 46.8519 | 0.51 | 3.0 | C | 89 | 60 | 43 | 334 | 54 | 142 | 210 | 4 | 305 | 50 |
| | 35 | CHAR | 2001/04/05 | 17:27:22 | −0.1086 | 46.212 | 14.31 | 3.0 | B | 213 | 60 | 121 | 343 | 42 | 48 | 281 | 10 | 173 | 62 |
| | 36 | CHMC | 2001/04/30 | 15:44:55 | 0.8982 | 46.9053 | 2.35 | 3.0 | B | 35 | 51 | −114 | 251 | 45 | −63 | 241 | 71 | 142 | 3 |
| | 37 | CHAR | 2001/06/08 | 13:26:53 | −1.0799 | 46.6625 | 11.76 | 5.2 | A | 123 | 86 | 139 | 216 | 49 | 5 | 175 | 22 | 73 | 28 |
| Armorican Massif | | | | | | | | | | | | | | | | | | | |
| | 38 | NAM | 1996/11/26 | 20:21:37 | −1.5227 | 48.6874 | 5.00 | 4.0 | A | 107 | 65 | 129 | 349 | 45 | 37 | 330 | 53 | 224 | 12 |
| | 39 | SAM | 1998/06/11 | 17:52:14 | −2.8011 | 47.6879 | 9.86 | 3.2 | C | 55 | 56 | 27 | 309 | 68 | 143 | 4 | 7 | 268 | 42 |
| | 40 | SAM | 1999/03/20 | 3:01:30 | −2.7934 | 47.6677 | 9.76 | 3.1 | D | 21 | 42 | 44 | 255 | 62 | 123 | 322 | 11 | 213 | 59 |
| | 41 | SAM | 1999/05/03 | 6:34:15 | −4.1686 | 47.8722 | 5.00 | 3.6 | B | 28 | 51 | 143 | 273 | 62 | −45 | 235 | 51 | 333 | 7 |
| | 42 | SAM | 2000/07/07 | 21:26:21 | −2.7256 | 47.3735 | 0.47 | 3.0 | C | 84 | 28 | −141 | 318 | 73 | −68 | 257 | 57 | 31 | 24 |
| | 43 | SAM | 2000/12/05 | 0:41:10 | −2.4996 | 47.9138 | 2.07 | 3.3 | B | 109 | 62 | 125 | 345 | 44 | 43 | 330 | 58 | 223 | 10 |
| | 44 | SAM | 2002/09/30 | 6:44:48 | −3.2457 | 47.8640 | 10.90 | 5.7 | A | 4 | 46 | −43 | 127 | 61 | −127 | 345 | 57 | 243 | 8 |

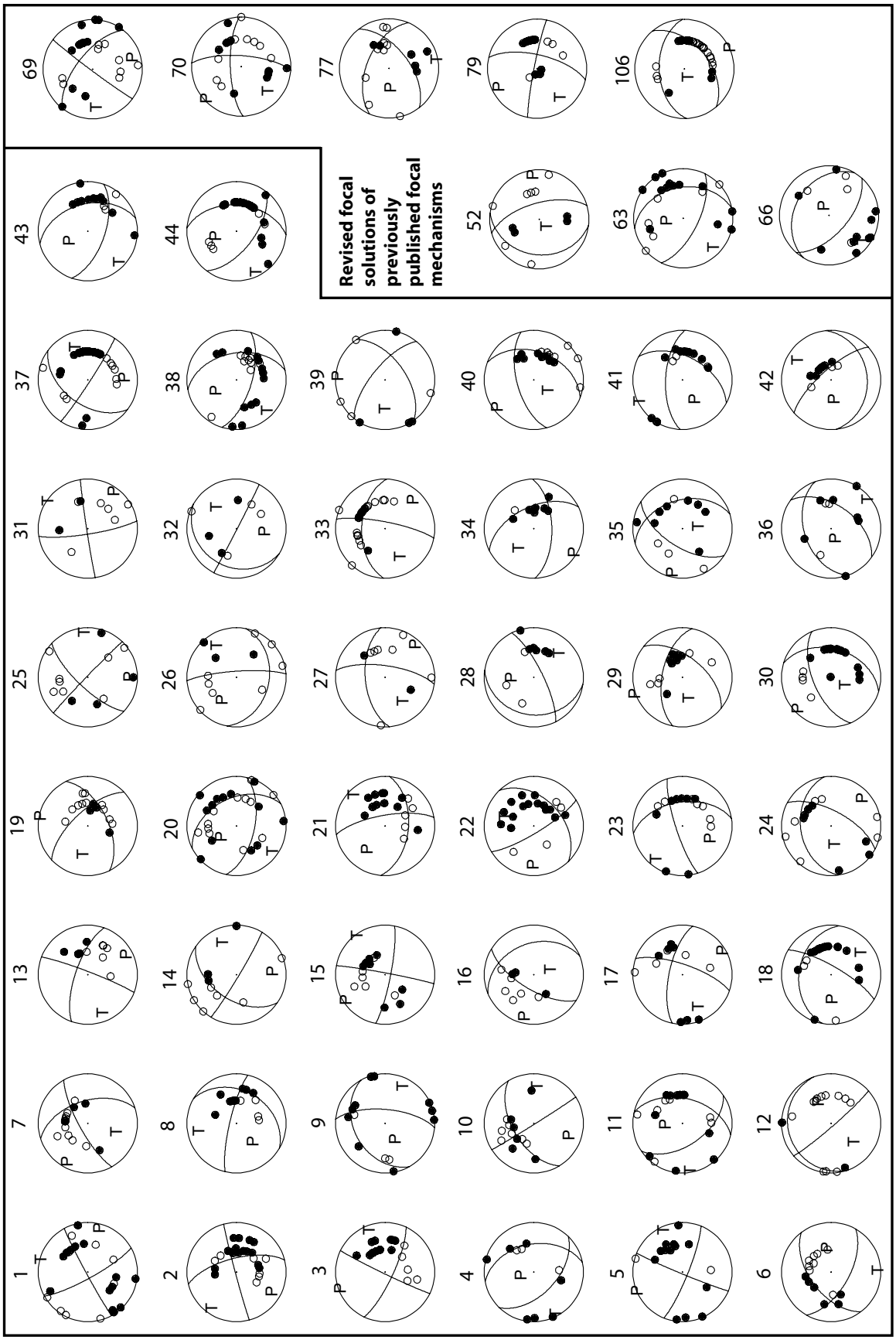


**Figure 5.** Focal mechanism solutions computed with the FPFIT software. Empty circle: dilatation, filled circle: compression. Some examples of revised focal mechanism solutions from previously published focal mechanisms are also presented (see Nicolas *et al.* 1990 for previous solutions)).

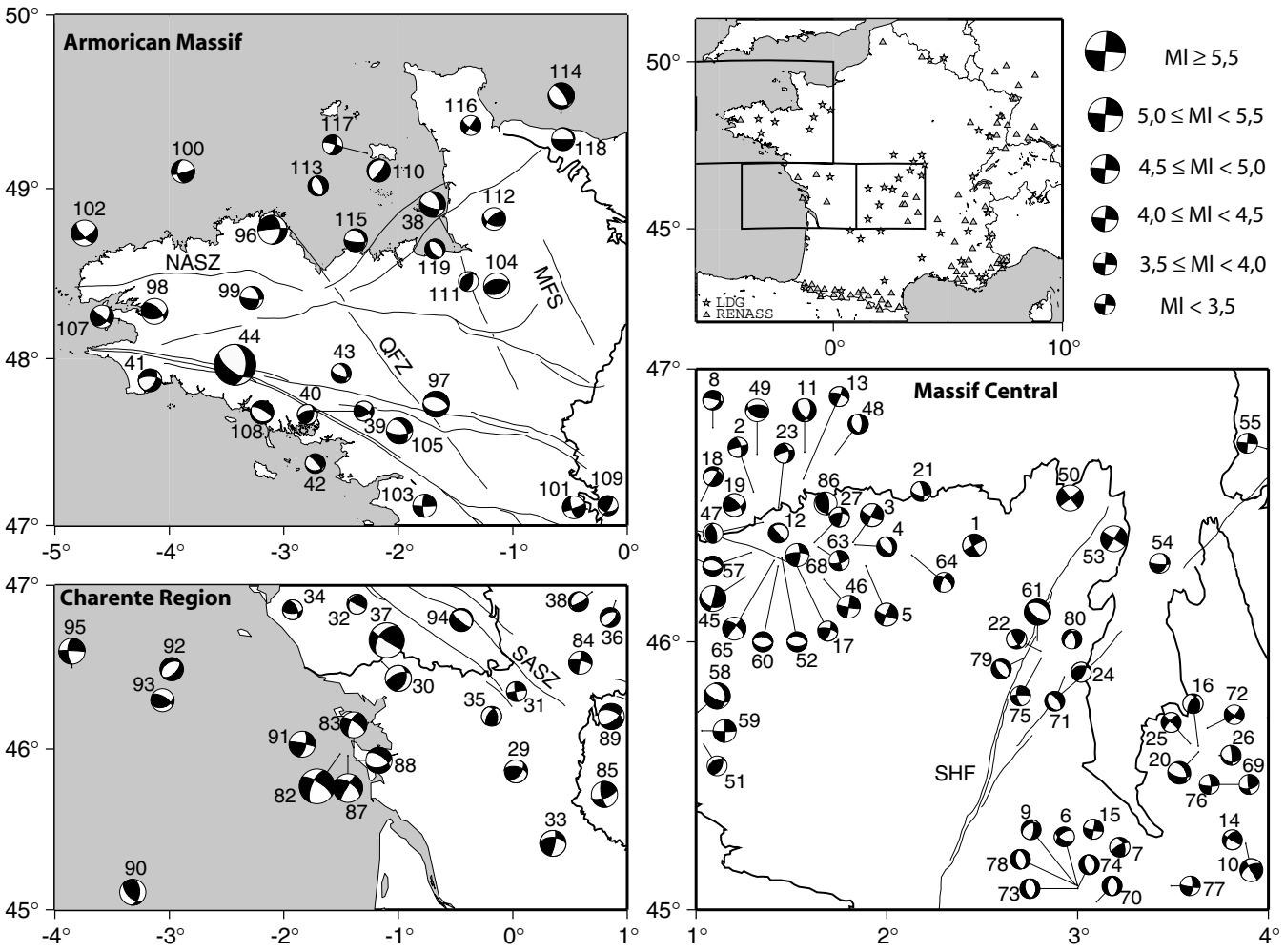


**Figure 6.** All focal mechanisms for the study area. Black (new focal mechanism) or grey (bibliographic focal mechanism) quadrants are compression, whereas white are dilatation. Grey stars are the seismic stations from the LDG network and grey triangles are the stations from the ReNaSS network. SASZ: South Armorican shear zone, NASZ: North Armorican shear zone, QFZ: Quessoy fault zone, MFS: Mayenne fault system, SHF: Sillon Houiller fault. (a) Armorican Massif, (b) Charente region, (c) Massif Central.

termination of the SASZ, a dextral strike-slip Hercynian ductile shear zone. In terms of the orientation of the *T*-axis, only a few focal mechanisms (N°: 28, 36, 89, 93) seem inconsistent with the other ones. Almost all are located in the northeast of Charente region and have a NW-trending *T*-axis, consistent with some mechanisms of the northwestern Massif Central. These mechanisms probably reflect a change in the stress field.

Fig. 6(c) shows the Massif Central, Charente and Armorican Massif focal mechanisms. We can observe that many focal mechanisms are concentrated in the northwestern Massif Central. This area is seismically more active than the southwestern Massif Central and EMC (Figs 2 and 4), with strong enough earthquakes ($M_L \geq 3.0$) to compute reliable focal mechanism solutions. The type of mechanism is variable; most mechanisms have an important strike-slip component and a NE-trending *T*-axis. In the southeastern Massif Central, 11 new focal mechanisms are presented. This area is characterized by a topographically high, north–south trending Quaternary volcanic range at 2.9 longitude east and the north–south Limagne graben from 3.0 to 3.7 longitude east.

## 5 INVERSION OF SEISMIC SLIP-VECTOR DATA SET TO DETERMINE THE STRESS STATE

### 5.1 Methodology

To compute the stress states responsible for present-day activity (i.e. for earthquakes) in the studied area, we perform quantitative inversions of the earthquake focal mechanisms, using the method proposed by Carey-Gailhardis & Mercier (1987, 1992), which is one of several existing algorithms (e.g. Vasseur *et al.* 1983; Gephart & Forsyth 1984). For a robust data set these different algorithms yield similar results (Mercier *et al.* 1991). Both the detailed methodology and the stress axis uncertainties are extensively presented in Baroux *et al.* (2001). The confidence of focal mechanism solutions is taken into account by the help of a weight given to the data, according to its quality, in the inversion procedure.

Taking into account the fact that very small magnitude events can only represent localmation, we have introduced a weight with regard

to the magnitude of events with focal mechanisms in our inversion. Our catalogue contains a significant number of events of magnitude higher than 4. We have verified that their focal mechanism solutions are in good agreement with the local stress tensor, inverted with the help of smaller magnitude events. Moreover, many other studies already point out that small magnitude events are generally responding to the same regional stress field as the largest events, thus we can statistically infer a good image of the regional stress field from them (Amelung & King 1997; Angelier *et al.* 2004).

### 5.2 Results

In the current study, we analyse 119 events including bibliographic (75, see references in Table 4) and new (44, Table 3) focal mechanisms. Delouis *et al.* (1993) directly inverted the polarities of 24 available earthquake focal solutions, from Nicolas *et al.* (1990) with the Rivera & Cisternas (1990) method. These authors determined the stress tensor of a wide area composed of the northern Massif Central, the Charente region and Armorican Massif. Nowadays, the densification of the seismic networks, together with the increased time of observation, allows us to compute reliable enough focal mechanism solutions, even for small-magnitude earthquakes ($M_L \geq 3$), and consequently permits us to examine smaller scale variations of the stress field. On the basis of the consistency of the focal mechanism *T*-axis orientations, we subdivide our focal mechanisms into five regionally significant data sets. These groups represent tectonic domains in which the stress field is expected to be rather homogeneous at the resolution allowed by our data. As all the events have been relocated, we have good confidence in the localization and correlation between the focal mechanism groups and the tectonic domains. Each focal mechanism located close to the boundary between two domains, and potentially compatible with both data sets, has been tested in each domain. It was then incorporated to the group with which it was the most compatible. During the inversion, a weight was given to each focal mechanism, according to its quality (Tables 3 and 4). The stress tensors computed by inversion of the focal mechanisms for the five areas are presented in Figs 7 and 8.

#### *5.2.1 Western Massif Central (WMC) and the Charente region (CHAR)*

For this zone, 46 mechanisms are available, including 18 new ones. Some bibliographic focal mechanism solutions are not well constrained because they occurred between 1976 and 1981, when the seismic networks were sparse. Thus, they were not used in the inversion. The inversion provides a well-constrained result, taking into account 38 out of 46 mechanisms, with more than 80 per cent of the ($\tau$, s) angular deviation below 20° and 100 per cent below 30°. It gives a strike-slip regime (vertical $\sigma_1$) with a horizontal 152°NE-trending $\sigma_2$ (Fig. 7).

#### *5.2.2 Eastern Massif Central (EMC)*

In southeastern Massif Central, we compute 12 new focal mechanisms. New focal mechanisms, together with the revised published solutions, furnish a set of 29 data points. Previously calculated events, from 1991, are recorded by dense and homogeneously distributed networks. Consequently, most mechanisms are well constrained, even if some small-magnitude events do not provide reliable focal mechanism solutions. Our focal mechanisms have been inverted together with 12 mechanisms published by Dorel *et al.* (1995). Dorel *et al.*'s focal mechanisms correspond to small earthquakes, with magnitudes ranging from 1.8 to 3.0, but have been computed using data from a temporary local network. The resultant stress regime is extensional and characterized by a 236°NE-trending $\sigma_3$. In a second stage, we combined this data set with the available focal mechanisms from the western Provence area, provided in Baroux *et al.* (2001) mainly around the Rhêne valley domain, at the southeast of the Massif Central. This combined data set of 34 mechanisms appears homogeneous (data being clearly compatible) and has been inverted. Some focal mechanism solutions are compressive and inconsistent with an extensional stress regime. Those solutions (e.g. n° 16) appear to be the less well constrained (see Tables 3 and 4) and are removed during the inversion process. This inversion leads to a reliable result, 21 focal planes out of 34 mechanisms were selected and more than 85 per cent of ($\tau$, s) angular deviations lower than 20° (Fig. 7). These selected planes are consistent with a WSW-trending extension (69°NE-$\sigma_3$). In the following, we will refer to this last result (Fig. 7).

#### *5.2.3 Northwestern Massif Central and northeastern Charente region (CHMC)*

Northwest of the Massif Central and southeast of the Armorican Massif, the focal mechanisms are characterized by SE-striking *T* axes, clearly inconsistent with the neighboring general NE-striking T-axis orientation. Eleven focal mechanisms are available in this area, seven of which are new and relatively well constrained. The poorly constrained events were removed from the inversion. The final inversion takes into account seven focal mechanisms and yields a good quality result with all ($\tau$, s) angular deviation below 10°. The stress tensor is extensional with a 130°NE-trending $\sigma_3$ (Fig. 7).

#### *5.2.4 Southern Armorican Massif (SAM)*

The Southern Armorican Massif (SAM) is characterized by the E-striking SASZ. Ten mechanisms, of which six are new, including the well-constrained 2001 September 30, $M_L = 5.7$ Lorient event (Perrot *et al.* 2005), have been inverted. The inversion result is of good quality and 7 of 10 mechanisms are well explained by the resulting stress field [all ($\tau$, s) angular deviation below 5°]. The stress tensor corresponds to an extensional stress regime and suggests a dominant normal-faulting regime with a non-trivial strike-slip component (Fig. 7). Some focal mechanism solutions are incompatible with extension (ex: n° 40). As in the other extensional zones, they are the less well constrained solutions (see Tables 3 and 4).

#### *5.2.5 Northern Armorican Massif (NAM)*

In Normandy (northeastern Armorican Massif), a regional network allowed Amorese *et al.* (2000) to publish reliable focal mechanism solutions for small-magnitude earthquakes. These focal mechanisms have been inverted together with newly computed solutions and revised older mechanisms (Nicolas *et al.* 1990).

Throughout the northern Armorican Massif (NAM), 13 of 19 focal mechanisms provide a reliable inversion with all ($\tau$, s) angular deviation below 20° (Fig. 7). The resultant stress regime appears to be complex, as the principal stress axes are not horizontal or vertical. We interpret this result as a stress field arising from the interaction of a dominant strike-slip regime and the attenuation of the extensional perturbation of the SAM.

**Table 4.** Bibliographic focal mechanisms. The focal mechanisms are classified by date for each geographical region. The stress field zone is determined *a posteriori* by stress field inversion.

| Geographical area | Number | Stess field zone | Date (YYYY/MM/DD) | Time (UTC) (HH/MM/SS) | Long. (°) | Lat. (°) | Depth (km) | Mag (Ml) | Quality | Plane A | | | Plane B | | | *P*-axis | | *T*-axis | | Ref. | R. |
|---|---|---|---|---|---|---|---|---|---|---|---|---|---|---|---|---|---|---|---|---|---|
| | | | | | | | | | | Az | Dip | Vect. | Az | Dip | Vect. | *P* az. | *P* dip. | *T* az. | *T* dip. | | |
| Central Massif | | | | | | | | | | | | | | | | | | | | | |
| | 45 | CHAR | 1968/04/07 | 19:13:23 | 1.29 | 46.21 | 7.5 | 4.0 | A | 14 | 85 | 125 | 111 | 363 | 9 | 316 | 40 | 76 | 31 | 2 | |
| | 46 | CHAR | 1975/04/13 | 4:56:29 | 1.66 | 46.25 | 12.0 | 3.5 | B | 10 | 89 | 0 | 100 | 84 | 180 | 325 | 5 | 55 | 3 | 2 | |
| | 47 | CHAR | 1976/05/20 | 3:15:38 | 1.35 | 46.44 | 2.0 | 2.9 | C | 160 | 68 | 57 | 40 | 39 | 143 | 274 | 17 | 28 | 55 | 2 | |
| | 48 | CHAR | 1976/08/18 | 16:02:54 | 1.72 | 46.69 | 14.0 | 3.1 | B | 2 | 58 | 105 | 155 | 35 | 67 | 310 | 73 | 81 | 12 | 2 | |
| | 49 | CHMC | 1976/10/22 | 18:46:27 | 1.32 | 46.69 | 7.0 | 3.5 | C | 265 | 53 | 64 | 124 | 44 | 120 | 13 | 5 | 115 | 69 | 2 | |
| | 50 | EMC | 1977/04/27 | 23:25:20 | 2.93 | 46.52 | 3.0 | 4.1 | A | 141 | 90 | 180 | 51 | 87 | 0 | 6 | 2 | 276 | 2 | 2 | |
| | 51 | CHAR | 1977/04/29 | 18:15:03 | 1.02 | 45.63 | 9.0 | 3.2 | C | 27 | 53 | 68 | 241 | 42 | 117 | 133 | 6 | 240 | 72 | 2 | |
| | 52 | CHAR | 1977/06/30 | 2:57:15 | 1.45 | 46.31 | 10.0 | 3.1 | C | 90 | 50 | 84 | 280 | 40 | 98 | 319 | 83 | 185 | 5 | 2 | ⋆ |
| | 53 | EMC | 1978/02/11 | 14:13:13 | 3.25 | 46.34 | 15.3 | 4.1 | A | 123 | 90 | 0 | 213 | 90 | 180 | 348 | 90 | 258 | 90 | 2 | |
| | 54 | EMC | 1978/03/30 | 17:33:39 | 3.43 | 46.29 | 5.0 | 3.3 | C | 20 | 35 | 19 | 94 | 79 | 123 | 158 | 27 | 38 | 45 | 1 | |
| | 55 | EMC | 1978/05/25 | 18:13:31 | 3.99 | 46.71 | 0.1 | 3.2 | C | 5 | 90 | 0 | 95 | 90 | 180 | 140 | 0 | 50 | 0 | 1 | |
| | 56 | EMC | 1978/08/29 | 22:23:48 | 3.29 | 43.69 | 8.0 | 4.1 | B | 32 | 57 | −80 | 230 | 34 | −105 | 272 | 76 | 129 | 12 | 2 | |
| | 57 | CHAR | 1978/09/03 | 3:51:36 | 1.30 | 46.32 | 5.0 | 3.1 | C | 90 | 50 | 80 | 285 | 41 | 101 | 308 | 81 | 187 | 5 | 2 | |
| | 58 | CHAR | 1978/11/06 | 10:48:24 | 1.01 | 45.70 | 12.0 | 4.4 | A | 74 | 43 | 150 | 187 | 70 | 51 | 305 | 16 | 54 | 49 | 2 | |
| | 59 | CHAR | 1979/05/11 | 18:06:25 | 1.03 | 45.64 | 13.4 | 3.5 | C | 0 | 89 | 0 | 90 | 84 | 180 | 315 | 5 | 45 | 3 | 2 | |
| | 60 | CHAR | 1981/09/28 | 3:58:45 | 1.41 | 46.24 | 15.7 | 3.3 | C | 93 | 43 | 85 | 280 | 47 | 95 | 246 | 86 | 7 | 2 | 2 | |
| | 61 | EMC | 1982/11/07 | 2:01:15 | 2.78 | 46.12 | 15.0 | 4.0 | A | 180 | 72 | 137 | 286 | 50 | 24 | 135 | 43 | 238 | 14 | 2 | |
| | 62 | EMC | 1984/02/19 | 21:14:37 | 5.54 | 43.42 | 8.0 | 4.3 | B | 226 | 44 | −153 | 336 | 72 | −49 | 204 | 47 | 95 | 17 | 2 | |
| | 63 | CHAR | 1985/02/11 | 7:06:01 | 1.64 | 46.32 | 14.1 | 3.4 | C | 75 | 70 | 3 | 344 | 87 | 160 | 298 | 16 | 31 | 12 | 2 | ⋆ |
| | 64 | CHAR | 1985/10/05 | 1:20:40 | 2.12 | 46.33 | 3.7 | 3.3 | C | 202 | 70 | 142 | 307 | 55 | 25 | 159 | 41 | 258 | 10 | 2 | |
| | 65 | CHAR | 1986/02/19 | 13:27:00 | 1.39 | 46.28 | 14.5 | 3.9 | B | 295 | 68 | 5 | 203 | 85 | 158 | 157 | 19 | 251 | 12 | 2 | |
| | 66 | EMC | 1986/02/25 | 17:10:39 | 4.72 | 43.95 | 5.0 | 3.6 | C | 203 | 43 | −102 | 7 | 48 | −79 | 212 | 82 | 105 | 3 | 2 | ⋆ |
| | 67 | EMC | 1987/02/05 | 9:59:37 | 4.56 | 43.66 | 5.0 | 3.5 | C | 356 | 72 | −67 | 230 | 29 | −140 | 236 | 57 | 104 | 24 | 2 | |
| | 68 | CHAR | 1987/04/29 | 13:57:09 | 1.51 | 46.28 | 10.3 | 3.7 | B | 268 | 71 | 177 | 359 | 87 | 19 | 132 | 11 | 225 | 16 | 2 | |
| | 69 | EMC | 1989/02/09 | 12:00:00 | 3.62 | 45.50 | 3.8 | 3.0 | C | 76 | 56 | 169 | 172 | 82 | 34 | 300 | 16 | 40 | 32 | 4 | ⋆ |
| | 70 | EMC | 1991/10/22 | 5:22:00 | 3.10 | 45.03 | 6.0 | 2.3 | C | 184 | 50 | 96 | 354 | 41 | 82 | 136 | 82 | 268 | 6 | 4 | ⋆ |
| | 71 | EMC | 1991/10/29 | 0:53:00 | 2.93 | 45.89 | 6.0 | 2.1 | C | 323 | 61 | 85 | 154 | 29 | 100 | 215 | 74 | 58 | 14 | 4 | |
| | 72 | EMC | 1991/10/31 | 3:13:00 | 3.65 | 45.59 | 4.2 | 2.0 | C | 38 | 80 | 174 | 129 | 82 | 10 | 352 | 13 | 264 | 2 | 4 | |
| | 73 | EMC | 1991/11/02 | 4:43:00 | 3.03 | 45.08 | 6.0 | 2.2 | C | 168 | 50 | 85 | 356 | 40 | 96 | 42 | 85 | 260 | 5 | 4 | |
| | 74 | EMC | 1991/11/04 | 11:54:00 | 3.00 | 45.08 | 6.0 | 2.7 | C | 168 | 50 | 85 | 354 | 40 | 96 | 55 | 85 | 262 | 5 | 4 | |
| | 75 | EMC | 1991/11/10 | 12:50:00 | 2.79 | 45.97 | 15.0 | 2.7 | C | 269 | 82 | 41 | 172 | 60 | 169 | 135 | 28 | 38 | 14 | 4 | |
| | 76 | EMC | 1991/12/15 | 7:05:00 | 3.71 | 45.49 | 7.1 | 2.3 | C | 92 | 75 | 19 | 357 | 75 | 164 | 314 | 22 | 224 | 2 | 4 | |
| | 77 | EMC | 1992/01/13 | 17:44:00 | 3.46 | 45.09 | 3.6 | 2.5 | C | 5 | 70 | 171 | 98 | 82 | 20 | 322 | 20 | 232 | 5 | 4 | ⋆ |
| | 78 | EMC | 1992/02/04 | 7:37:00 | 3.03 | 45.08 | 4.1 | 2.4 | C | 346 | 44 | 84 | 174 | 48 | 96 | 148 | 85 | 259 | 3 | 4 | |
| | 79 | EMC | 1992/02/06 | 16:55:00 | 2.68 | 45.97 | 5.1 | 2.1 | C | 315 | 36 | 80 | 147 | 56 | 97 | 84 | 80 | 231 | 9 | 4 | ⋆ |
| | 80 | EMC | 1992/03/06 | 0:49:00 | 2.98 | 46.01 | 2.6 | 1.8 | C | 347 | 60 | 53 | 223 | 35 | 136 | 222 | 68 | 92 | 12 | 4 | |
| | 81 | EMC | 1998/02/09 | 14:16:56 | 4.89 | 43.90 | 6.0 | 3.1 | C | 24 | 73 | −78 | 239 | 21 | −123 | 277 | 60 | 123 | 27 | 5 | |

**Table 4** (*Continued.*)

| Geographical area | Number | Stress field zone | Date (YYYY/MM/DD) | Time (UTC) (HH/MM/SS) | Long. (°) | Lat. (°) | Depth (km) | Mag (Ml) | Quality | Plane A | | | Plane B | | | *P* Axis | | *T* Axis | | Ref. | R. |
|---|---|---|---|---|---|---|---|---|---|---|---|---|---|---|---|---|---|---|---|---|---|
| | | | | | | | | | | Az | Dip | Vect. | Az | Dip | Vect. | *P* az. | *P* dip. | *T* az. | *T* dip. | | |
| Charente region | | | | | | | | | | | | | | | | | | | | | |
| | 82 | CHAR | 1972/09/07 | 22:26:56 | −1.26 | 46.05 | 10.0 | 5.2 | B | 303 | 70 | 27 | 203 | 65 | 158 | 164 | 33 | 72 | 4 | 2 | |
| | 83 | CHAR | 1972/09/08 | 1:51:51 | −1.45 | 45.95 | 10.0 | 4.1 | B | 303 | 70 | 27 | 203 | 65 | 158 | 164 | 33 | 72 | 4 | 2 | |
| | 84 | CHAR | 1975/12/28 | 2:16:07 | 0.594 | 46.45 | 12.0 | 3.9 | C | 190 | 87 | 162 | 281 | 74 | 3 | 144 | 14 | 237 | 9 | 2 | |
| | 85 | CHAR | 1976/09/08 | 19:54:41 | 0.89 | 45.61 | 15.0 | 4.3 | B | 168 | 71 | 22 | 70 | 68 | 159 | 299 | 2 | 30 | 30 | 2 | |
| | 86 | CHAR | 1977/04/06 | 11:09:33 | 1.68 | 46.51 | 6.0 | 3.5 | B | 131 | 23 | 48 | 335 | 69 | 106 | 260 | 65 | 58 | 24 | 2 | |
| | 87 | CHAR | 1977/10/10 | 6:05:56 | −1.43 | 45.96 | 5.0 | 4.7 | B | 305 | 60 | 8 | 211 | 83 | 150 | 164 | 26 | 262 | 16 | 2 | |
| | 88 | CHAR | 1978/05/27 | 7:47:40 | −1.37 | 45.93 | 10.0 | 4.1 | B | 305 | 57 | 121 | 77 | 44 | 51 | 269 | 63 | 13 | 7 | 2 | |
| | 89 | CHMC | 1983/04/21 | 1:53:08 | 0.99 | 46.18 | 5.0 | 4.0 | A | 122 | 85 | 31 | 29 | 60 | 174 | 252 | 17 | 350 | 25 | 2 | |
| | 90 | CHAR | 1983/05/08 | 17:47:51 | −3.26 | 45.05 | 15.0 | 4.0 | B | 5 | 46 | 130 | 135 | 56 | 57 | 248 | 6 | 349 | 62 | 2 | |
| | 91 | CHAR | 1984/02/25 | 6:08:20 | −1.75 | 46.02 | 10.0 | 4.2 | B | 300 | 70 | 50 | 188 | 44 | 151 | 166 | 49 | 58 | 15 | 2 | |
| | 92 | CHAR | 1984/04/08 | 7:20:21 | −2.98 | 46.47 | 8.8 | 3.9 | C | 45 | 54 | 81 | 240 | 37 | 102 | 281 | 79 | 141 | 9 | 2 | |
| | 93 | CHAR | 1984/06/07 | 16:27:22 | −3.09 | 46.30 | 10.0 | 3.8 | C | 302 | 64 | 121 | 68 | 40 | 43 | 10 | 13 | 257 | 59 | 2 | |
| | 94 | CHAR | 1985/10/07 | 13:01:49 | −0.42 | 46.80 | 11.0 | 3.9 | C | 130 | 76 | 92 | 300 | 14 | 80 | 43 | 59 | 218 | 31 | 2 | |
| | 95 | CHAR | 1986/03/22 | 2:30:28 | −3.83 | 46.50 | 20.0 | 4.1 | B | 272 | 86 | 27 | 180 | 70 | 176 | 138 | 17 | 44 | 12 | 2 | |
| Armorican Massif | | | | | | | | | | | | | | | | | | | | | |
| | 96 | NAM | 1975/08/30 | 14:07:49 | −3.11 | 48.85 | 3.0 | 4.5 | B | 265 | 85 | 135 | 360 | 45 | 7 | 213 | 33 | 320 | 25 | 2 | |
| | 97 | SAM | 1978/02/12 | 18:34:05 | −1.67 | 47.73 | 2.0 | 4.1 | B | 92 | 42 | 77 | 289 | 49 | 101 | 260 | 81 | 11 | 3 | 2 | |
| | 98 | NAM | 1978/09/20 | 15:40:40 | −4.13 | 48.28 | 15.0 | 4.0 | B | 312 | 62 | −124 | 77 | 43 | −44 | 18 | 11 | 271 | 58 | 2 | |
| | 99 | NAM | 1979/01/13 | 15:38:02 | −3.28 | 48.36 | 7.0 | 3.9 | C | 95 | 80 | 53 | 352 | 38 | 164 | 330 | 43 | 213 | 26 | 2 | |
| | 100 | NAM | 1981/06/20 | 0:34:57 | −3.82 | 49.06 | 8.7 | 3.7 | C | 75 | 79 | 137 | 175 | 48 | 15 | 26 | 37 | 131 | 19 | 2 | |
| | 101 | CHMC | 1981/08/31 | 6:14:29 | −0.37 | 47.09 | 8.0 | 3.5 | C | 163 | 70 | 9 | 70 | 82 | 160 | 25 | 20 | 118 | 8 | 2 | |
| | 102 | NAM | 1981/09/04 | 4:42:01 | −4.62 | 48.64 | 16.0 | 4.2 | B | 139 | 70 | 150 | 60 | 62 | 23 | 11 | 5 | 277 | 35 | 2 | |
| | 103 | SAM | 1982/11/09 | 13:44:46 | −1.77 | 47.06 | 16.0 | 3.9 | C | 90 | 86 | −166 | 181 | 76 | −4 | 136 | 7 | 45 | 13 | 2 | |
| | 104 | NAM | 1983/07/07 | 3:52:24 | −1.11 | 48.41 | 9.0 | 4.2 | B | 60 | 42 | −73 | 262 | 50 | −105 | 342 | 4 | 232 | 78 | 2 | |
| | 105 | SAM | 1983/08/14 | 15:35:51 | −1.99 | 47.57 | 4.0 | 4.0 | B | 90 | 65 | 50 | 333 | 46 | 144 | 312 | 52 | 208 | 11 | 2 | |
| | 106 | CHAR | 1985/09/30 | 11:16:32 | 1.29 | 47.45 | 18.6 | 4.7 | A | 50 | 49 | 63 | 268 | 48 | 118 | 159 | 1 | 251 | 70 | 2 | ⋆ |
| | 107 | NAM | 1987/01/10 | 0:51:15 | −4.57 | 48.24 | 15.0 | 3.8 | C | 129 | 86 | 45 | 35 | 45 | 174 | 1 | 32 | 254 | 25 | 2 | |
| | 108 | SAM | 1987/01/15 | 14:21:15 | −3.11 | 47.67 | 11.3 | 3.7 | C | 110 | 21 | 81 | 300 | 69 | 94 | 216 | 65 | 27 | 24 | 2 | |
| | 109 | CHMC | 1987/03/05 | 23:09:07 | −0.15 | 47.12 | 7.0 | 3.3 | C | 100 | 40 | −155 | 30 | 74 | −53 | 261 | 48 | 147 | 20 | 2 | |
| | 110 | NAM | 1990/04/30 | 23:35:57 | −2.1 | 49.10 | 10.8 | 3.5 | C | 35 | 75 | 90 | 215 | 15 | 90 | 305 | 60 | 125 | 30 | 3 | |
| | 111 | NAM | 1990/11/08 | 18:21:47 | −1.49 | 48.49 | 8.6 | 3.0 | C | 15 | 58 | −70 | 230 | 37 | −119 | 121 | 11 | 246 | 71 | 3 | |
| | 112 | NAM | 1993/07/26 | 18:52:21 | −1.11 | 48.77 | 7.8 | 3.5 | C | 115 | 45 | −150 | 227 | 69 | −49 | 346 | 14 | 93 | 49 | 3 | |
| | 113 | NAM | 1994/09/17 | 6:05:03 | −2.7 | 49.01 | 8.0 | 3.4 | C | 160 | 35 | 90 | 340 | 55 | 90 | 250 | 80 | 70 | 10 | 3 | |
| | 114 | NAM | 1994/11/30 | 16:31:21 | −0.57 | 49.44 | 14.0 | 4.1 | B | 105 | 25 | 50 | 328 | 71 | 107 | 262 | 60 | 45 | 24 | 3 | |
| | 115 | NAM | 1995/04/22 | 13:10:13 | −2.35 | 48.62 | 9.5 | 3.5 | C | 95 | 75 | 70 | 330 | 25 | 142 | 340 | 56 | 201 | 27 | 3 | |
| | 116 | NAM | 1996/06/01 | 12:29:23 | −1.32 | 49.35 | 7.5 | 3.0 | C | 125 | 70 | 180 | 35 | 90 | 0 | 348 | 14 | 82 | 14 | 3 | |
| | 117 | NAM | 1997/06/22 | 16:50:16 | −2.27 | 49.20 | 13.1 | 3.4 | C | 285 | 80 | 158 | 19 | 68 | 11 | 240 | 21 | 333 | 7 | 3 | |
| | 118 | NAM | 1998/08/08 | 10:36:16 | −0.55 | 49.25 | 4.9 | 3.5 | C | 91 | 85 | 78 | 339 | 13 | 157 | 348 | 49 | 192 | 39 | 3 | |
| | 119 | NAM | 1998/12/07 | 0:23:28 | −1.65 | 48.58 | 9.9 | 3.3 | C | 150 | 55 | 100 | 313 | 36 | 76 | 94 | 77 | 233 | 9 | 3 | |

References: (1) Santoire (1976), (2) Nicolas *et al.* (1990), (3) Amorese *et al.* (2000), (4) Dorel *et al.* (1995), (5) Baroux *et al.* (2001).
Revised focal mechanism solutions are marked with a star.

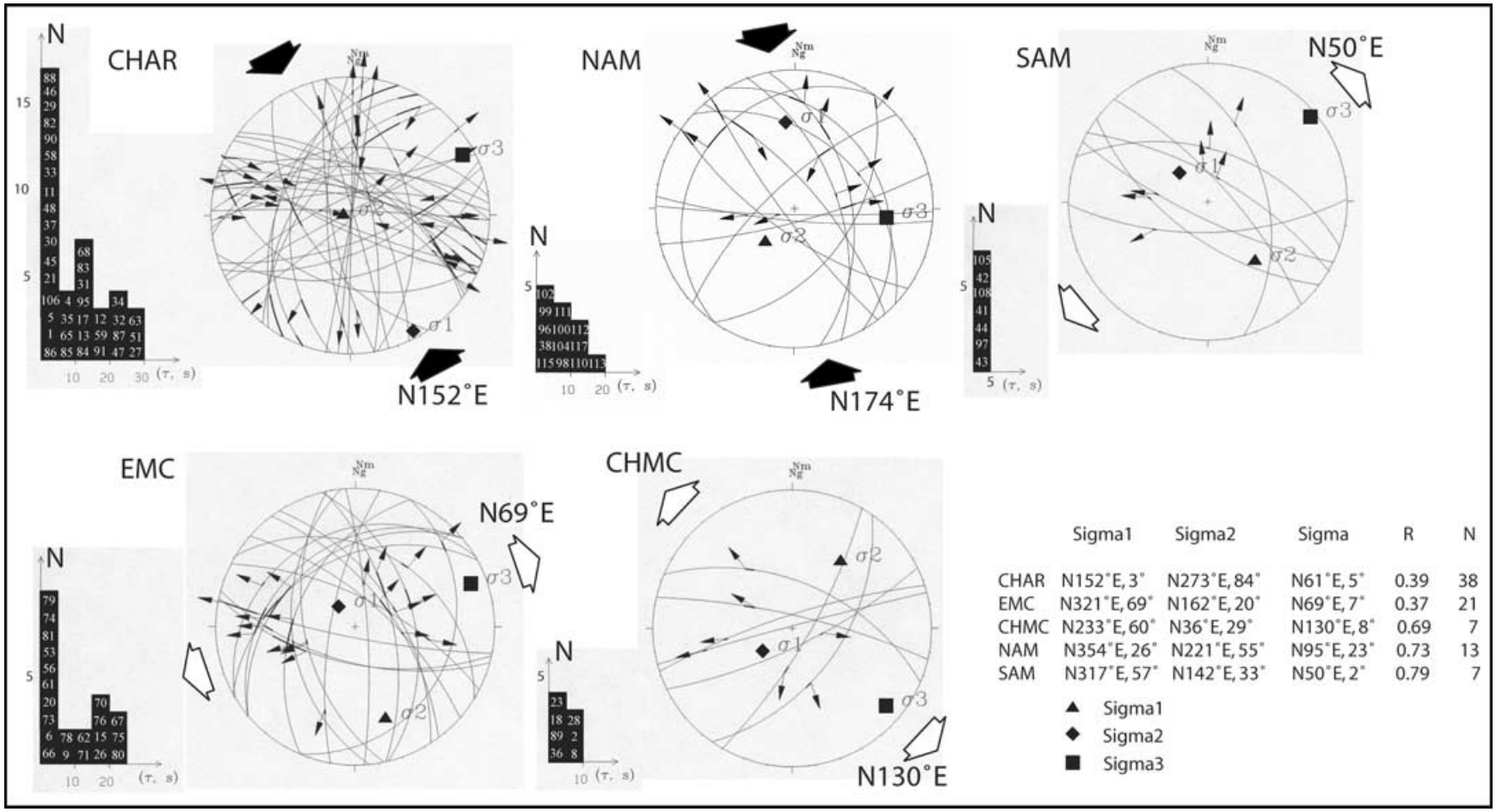


| | Sigma1 | Sigma2 | Sigma | R | N |
|---|---|---|---|---|---|
| CHAR | N152°E, 3° | N273°E, 84° | N61°E, 5° | 0.39 | 38 |
| EMC | N321°E, 69° | N162°E, 20° | N69°E, 7° | 0.37 | 21 |
| CHMC | N233°E, 60° | N36°E, 29° | N130°E, 8° | 0.69 | 7 |
| NAM | N354°E, 26° | N221°E, 55° | N95°E, 23° | 0.73 | 13 |
| SAM | N317°E, 57° | N142°E, 33° | N50°E, 2° | 0.79 | 7 |

**Figure 7.** Stress tensors computed for the five areas projected on a lower hemisphere Wulff diagram. Small arrows indicate slip vectors, large white arrows are extension and large black arrows are compression directions. Histograms are the number of focal mechanisms ($N$) versus the ($\tau$, s) angular deviation, in degrees. Black triangle: $\sigma_1$, diamond: $\sigma_2$, square: $\sigma_3$.

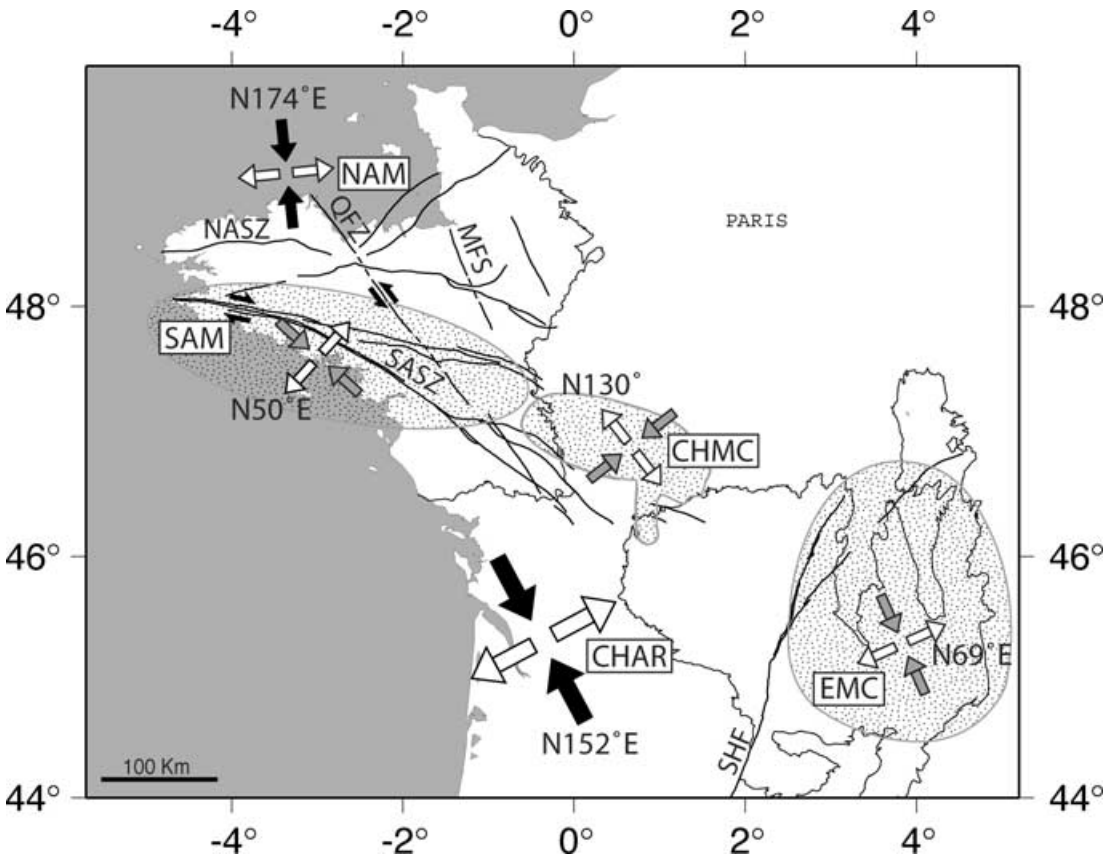


**Figure 8.** Stress tensors of the different areas. Black arrows indicate the direction of the maximum horizontal compression ($\sigma_{\mathrm{Hmax}}$), white arrows indicate the direction of the minimum horizontal compression ($\sigma_{\mathrm{hmin}}$). Dotted areas circled in grey represent the regional extent of a particular stress field. NAM: North Armorican Massif, SAM: South Armorican Massif, CHMC: northeastern Charente and northwestern Massif Central, CHAR: western Massif Central and the Charente region, EMC: eastern Massif Central. SASZ: South Armorican shear zone, NASZ: North Armorican shear zone, QFZ: Quessoy fault zone, MFS: Mayenne fault system, SHF: Sillon Houiller fault.

## 6 INTERPRETATION OF THE RESULTS

### 6.1 Effect of the mantle plume

The EMC zone, is characterized by an extensional stress state, confirming the results of hydraulic tests in boreholes from Cornet & Burlet (1992), and the conclusions of Delouis *et al.* (1993) and Dorel *et al.* (1995), based on focal mechanisms analysis. Our study shows that the extension in the Massif Central is limited by the SHF in the west. Extension is probably related to the ascent of the hot mantle plume located beneath this area, that is inferred from teleseismic tomography (Granet *et al.* 1995a,b). The plume is believed to be the origin of an anomalous thermal regime of the crust related to volcanism (Vasseur 1982; Lucazeau *et al.* 1984; Lucazeau & Vasseur 1989). We propose that the extensional deviatoric stress is the result of bulging of the crust at the apex of the hot mantle plume. This implies that the SHF is acting as a passive boundary between the EMC and WMC. Thus, we infer a lithospherical scale to this fault. Inspection of digital elevation models (DEM) provides evidence that the eastern, volcanic, part of the Massif is uplifted with respect to the western part. On the basis of high-resolution DEM analysis, rivers and lava flows across faults, and the distribution and timing of sedimentation, Michon & Merle (2001) deduce a normal displacement along the SHF and associated faults that accommodate Quaternary uplift of the EMC.

Southeast of the Massif Central, Baroux *et al.* (2001) have shown that the Rhêne valley is actively in extension. These authors suggest that this extension is probably the result of the influence of the extensional stress regime of the Massif Central that they relate to the mantle plume. Focal mechanism inversions, in the present study, also show that the stress regime of the EMC and the Rhêne valley are consistent, confirming that extension in these two regions might have the same origin, namely the effect of the mantle plume.

### 6.2 Effect of plate and microplate tectonics

Alternatively, the observed stress perturbation could be related to intraplate forces. For instance, the anticlockwise rotation of Iberian microplate with regard to Eurasia and/or incipient subduction in the Bay of Biscay generates intraplate forces from which the deformation of the Pyrenees chain and the Bay of Biscay are the most clear expressions. In the west of our study area, the opening of the Bay of Biscay has accommodated the rotation of Iberia from its beginning at Aptian time, 114 Ma (Montardet *et al.* 1979; Olivet 1996). Nowadays, no large earthquakes are recorded offshore in the Bay of Biscay. Small earthquakes might occur but are not detected by French, Spanish and Portuguese networks. Accumulation of extensional stress on the SASZ or subparallel structures could be responsible for the $M_{\mathrm{L}} > 5.0$ earthquakes that appear to be distributed all along

the Atlantic coast, following the fault zones (Fig. 6). NE–SW extensional stress in the SAM zone generates extension with a small dextral component on the northern part of the SASZ. As the southern branch of the SASZ is striking more N–S in the CHAR, the strike-slip component becomes more important. Forces associated with the rotation of Iberia generate, towards the North, compressional stress in the east and extensional stress in the west. In the east, the compressional stresses are accommodated by deformation of the Pyrenees. Thus, at the longitude of the northwestern Massif Central, the stress induced by the rotation of Iberia is null, because it is released in the eastern Pyrenees. Extension in CHMC ($\sigma_{\mathrm{hmin}}$ striking 132°NE) is parallel to the strike of the fan-shaped eastern termination of the SASZ, which strikes from ∼120°NE to ∼130°NE.

The coeval influence of Europe–Africa convergence and rotation of Iberia on pre-existing zones of weakness (mainly the SASZ), and the effect of the mantle plume beneath the Central Massif should partly explain the regional NW–SE compression and the short scale variations of the stress field computed by the inversion of focal mechanisms.

## 7 DISCUSSION

(i) Refinement of the image of the seismicity of western and central France, a slowly deforming intraplate region, has been accomplished by synthesis of seismological bulletins from different networks and the location of 4574 events. Earthquakes have then been relocated by joint hypocentres and velocity structure inversion. The new epicentre distribution points out that the seismicity of those regions is much less diffuse than it was previously thought. For instance, in the Massif Central, most events are aggregated in clusters. These clusters are concentrated in the most tectonically active parts of the Massif: along the north–south volcanic area, south of the Limagne graben and in the northwesternmost part of the Massif, where the SASZ is merging with the SHF. In western France, the epicentre distribution has been improved but it is still diffuse.

(ii) The computation of 44 new focal mechanisms and revision of some bibliographic solutions allow a better comprehension of the strain and stress distribution. The inversion of 119 focal mechanisms in central and western France illustrates the dependence of the resolution of the stress field on the amount and spatial distribution of the data. In 1993, over the same area, Delouis *et al.* only had 16 mechanisms available for analysis. Their result corresponds to an average stress field of the area ($\sigma_1$ close to the vertical, $\sigma_2$ horizontal and striking 125°NE, and $\sigma_3$ close to the horizontal and striking 35°NE), as the extensional focal mechanisms were not inverted separately. The local to regional size extensional zones defined by our study require a sufficient amount of data to be sampled. In theory, four mechanisms are enough to be inverted as we determine four parameters ($\sigma_1$, $\sigma_2$, $\sigma_3$ and $R$) during the inversion, but a minimum of six mechanisms is desirable. As opposed to hydraulic tests, the focal mechanisms do not provide direct measurements of the stress field. Several mechanisms must be inverted together, thus a computed stress field does not correspond to a single point but to data that encompass a larger region. The presence of local perturbations of the stress field can then introduce a bias in the inversion if all mechanisms are inverted together. Therefore, when direct measurements of the stress field are available in slowly deforming regions, a mismatch between the measured and computed stress field can indicate the presence of local perturbations of the stress field. Indeed, this study allows us to characterize two kinds of stress regimes, regional strike-slip versus local extensional.

(iii) The regional stress field in the study domain approximately agrees with the model configurations of Gölke & Coblentz (1996), relating it to the joint effect of the convergence of Africa and Europe and of the Mid-Atlantic ridge push. The extensional stress field corresponds to three perturbations of the regional stress field. We propose that they are the result of inherited lithospherical faults undergoing plate boundary and intraplate forces. Those plate boundary and intraplate forces originate from the convergence of Africa and Europe and the Mid-Atlantic ridge push, and by the rotation of the Iberian microplate, respectively. In the Massif Central, the SHF plays the role of a lithospheric scale barrier (i.e. passive boundary) between a western domain and an eastern domain uplifted by the thermal effect of a mantle plume at the base of the lithosphere

(iv) For the Provence area, Baroux *et al.* (2001) suggest that 'abrupt spatial stress changes in a narrow zone could reflect a tectonic model with upper crustal fragments (blocks) decoupled from the lithospheric mantle by the ductile lower crust as suggested by Müller *et al.* (1997) for short-scale variation of the tectonic regimes acting in western Europe'. In Provence, these authors observed stress field variations over a distance range of tens of kilometres. In our study area, the stress field variations have a minimum wavelength of more than 100 km, three times the crustal thickness. These variations are related to lithospheric rather than crustal scale processes, as proposed by Bonnet *et al.* (2000) for the development of relief in the Armorican Massif. Furthermore, the major structures influencing the stress field are of lithospheric scale (the SASZ and the SHF). Another argument to link these perturbations to lithospheric processes is the correlation between the geographic areas of stress perturbation and lateral variation of *Pn* anisotropy beneath France, as computed by Juhenderc & Granet (1999). The upper-mantle seismic anisotropy is believed to arise from preferred orientation of olivine grains, which are responding to the stress field during mantle deformation. Correlation between the true direction of anisotropy and crustal stress does not make it necessary to invoke decoupling of the crust in our study area. Nevertheless, east of the SHF, the extensional regime associated with high heat flow values ($>100\,\mathrm{mW\,m^{-2}}$) could favour crustal decoupling. If crustal decoupling does occur, we believe that it is restricted in area to the extension of the thermal influence of the mantle plume: that is to say, the Massif Central east of the SHF, the Rhêne valley and the Provence region.

## 8 CONCLUSION

(i) Synthesis of seismological bulletins from different networks and the location of 4574 events, and precise relocation by joint hypocentres and velocity structure inversion allows improvement of the image of the seismicity of western and central France.

(ii) Taking into account the improvement in the hypocentral location of the events and in the velocity model, we computed realistic take-off angles. Then, we determined 44 new focal mechanism solutions and we revised the previously published focal mechanisms in order to construct a set of 119 homogeneously computed focal mechanisms.

(iii) The inversion of these focal mechanisms allows us to recognize a regional NW–SE compression. The regional strike-slip stress field appears to be overprinted by three local extensional perturbations. These are located in the EMC, in the SAM and at the southern termination of the SASZ, between the two massifs.

(iv) The stress field perturbations are of lithospherical scale and correlate with the lateral variation of *Pn* anisotropy, which is an

indirect consequence of stress orientation in the mantle. Thus, it is not necessary to invoke decoupling of the crust in our study area, as previous authors have suggested (Müller *et al.* 1997). If crustal decoupling does occur, we believe that it is restricted in area to the extension of the thermal influence of the mantle plume: that is to say, the Massif Central east of the SHF, the Rhêne Valley and the Provence region.

(v) Following Gölke & Coblentz (1996), we relate the regional strike-slip stress field to the joint effect of Europe–Africa convergence and Mid-Atlantic ridge push. We propose that the extensional deviatoric stress in the EMC is the result of the bulging of the crust at the apex of the hot mantle plume. The two other extensional areas approximately follow the SASZ. We argue in favour of intraplate extensional stress acting on pre-existing weak zones, and we relate those forces to the anticlockwise rotation of the Iberian microplate and/or incipient subduction in the Bay of Biscay.

## ACKNOWLEDGMENTS

This work was made possible thanks to the data provided by the Réseau National de Surveillance Sismique (ReNaSS), the Instituto Geografico National (IGN) and the SISMALP network. Data from the SISCAEN network were also provided by Daniel Amorèse. We are grateful to Marc Nicolas and Bertrand Delouis for providing their polarity data. We are also grateful to C. Gélis for her help in the development of a subroutine. We thank Professor Diane Doser and an anonymous reviewer for their enhancing comments. This work is contribution number 670 of UMR 6526 Géosciences Azur.

## REFERENCES

Amelung, F. & King, G., 1997. Large-scale tectonic deformation inferred from small earthquakes, *Nature,* **386**, 702–705.

Amorese, D., Walker, A., Lagarde, J.-L., Santoire, J.-P., Volant, P., Font, M. & Lecornu, M., 2000. New seismotectonic data from an intraplate region: focal mechanisms in the Armorican Massif (northwestern France), *Geophys. J. Int.,* **143**, 837–846.

Angelier, J., Slunga, R., Bergerat, F., Stefansson, R. & Homberg, C., 2004. Perturbation of stress and oceanic rift extension across transform faults shown by earthquake focal mechanisms in Iceland, *Earth planet. Sci. Lett.,* **219**, 271–284.

Ayarza, P., Martinez Catalan, J.R., Alvarez-Marron, J., Zeyen, H. & Juhlin, C., 2004. Geophysical constraints on the deep structure of a limited ocean-continent subduction zone at the north Iberian Margin, *Tectonics,* **23**, 1 (TC1010).

Baroux, E., Béthoux, N. & Bellier, O., 2001. Analyses of the stress field in southeastern France from earthquakes focal mechanisms, *Geophys. J. Int.,* **145**, 336–348.

Bonnet, S., Guillocheau, F., Brun, J.-P. & Van Den Driessche, J., 2000. Large-scale relief developpement related to quaternary tectonic uplift of a Proterozoic-Paleozoic basement: The Armorican Massif, NW France, *J. geophys. Res.,* **105**, 19 273–19 288.

Carey-Gailhardis, E. & Mercier, J.-L., 1987. A numerical method for determining the state of stress using focal mechanisms of earthquake populations: application to Tibetan teleseisms and microseismicity of Southern Peru, *Earth planet. Sci. Lett.,* **82**, 165–179.

Carey-Gailhardis, E. & Mercier, J.-L., 1992. Regional state of stress, fault kinematics and adjustments of blocks in a fractured body of rock: application to the microseismicity of the Rhine graben, *J. Struct. Geol.,* **14(8/9)**, 1007–1017.

Cornet, F.H. & Burlet, D., 1992. Stress field determinations in France by hydrolic tests in boreholes, *J. geophys. Res.,* **97**, 11 829–11 849.

Delhaye, A., 1976. Etude de la sismicité récente de la région d'Oléron, *PhD thesis*, Université de Paris VI, Paris, p. 80.

Delouis, B., Haessler, H., Cisternas, A. & Rivera, L., 1993. Stress tensor determination in France and neighbouring regions, *Tectonophysics,* **221**, 413–437.

Dorel, J., Fourvel, D. & Donnedieu, G., 1995. Etude de la sismicité de l'Auvergne et des régions limitrophes (Massif central français), *Bull. geol. Soc. Fr.,* **166**, 271–284.

Ellsworth, J.D., 1977. Three-dimensional structure of the crust and mantle beneath the island of Hawaii, *PhD thesis*, Mass. Inst of Technol. Cambridge, MA.

Froidevaux, C., Brousse, R. & Bellon, H., 1974. Hot spot in France?, *Nature,* **248**, 749–751.

Geiger, L., 1910. Herdbestimmung bei Erdbeben aus den Ankunfzeiten, K Gessel, *Wiss. Gott.,* **4**, 331–349.

Gephart, J.W. & Forsyth, W.D., 1984. An iproved method for determining the regional stress tensor using earthquake focal mechanism data:Application to the San Fernando earthquake sequence, *J. geophys. Res.,* **89**, 9305–9320.

Gölke, M. & Coblentz, D., 1996. Origins of the European regional stress field, *Tectonophysics,* **266**, 11–24.

Granet, M., Wilson, M. & Achauer, U., 1995a. Imaging a mantle plume beneath the French Massif Central, *Earth Planet. Sci. Lett.,* **136**, 281–296.

Granet, M., Stoll, G., Dorel, J., Achauer, U., Poupinet, G. & Fuchs, K., 1995b. Massif Central (France): new constraints on the geodynamical evolution from teleseismic tomography, *Geophys. J. Int.,* **121**, 33–48.

Grünthal, G. & Stromeyer, D., 1992. The recent crustal stress field in central Europe: trajectories and finite element modelling, *J. geophys. Res.,* **97**, 11 805–11 820.

Juhenderc, S. & Granet, M., 1999. Two-dimensional anisotropic tomography of lithosphere beneath France using regional arrival times, *J. geophys. Res.,* **104**, 13 201–13 215.

Kissling, E., Ellsworth, W.L. & Cockerham, R.S., 1984. Three-dimensional structure of the Long Valley Caldera, California region, by geotomography, *US Geol Surv.Open File Rep.,*84-939, 188–220.

Kissling, E., Ellsworth, W.L., Eberhart-Phillips, D. & Kradolfer, U., 1994. Initial reference models in local earthquake tomography, *J. geophys. Res.,* **99**, 19 635–19 646.

Lee, W.H.K. & Lahr, J.C., 1975. HYPO71 (revised): a computer program for determining hypocenter, magnitude and first motion pattern of local earthquakes, *US Geol Surv.Open File Rep.,*75-311, 1–116.

Lucazeau, F. & Vasseur, G., 1989. Heat flow density data from France and surrounding margins, *Tectonophysics,* **164**, 251–258.

Lucazeau, F., Vasseur, G. & Bayer, R., 1984. Interpretation of heat flow data in the french Massif Central, *Tectonophysics,* **103**, 99–119.

Mazabraud, Y., Béthoux, N. & Deroussi, S., 2005. Characterisation of the seismological pattern in a slowly deforming intraplate region: central and western France, *Tectonophysics,* submitted.

Mercier, J.L., Carey-Gailhardis, E. & Sébrier, M., 1991. Paleostress determinations from fault kinematics: application to the neotectonics of the Hymalaya-Tibet and the Central Andes, *Phil. Trans. R. Soc. Lond., A.,* **337**, 41–52.

Merle, O. & Michon, L., 2001. The formation of the West European rift: a new model as exemplified by the Massif Central area, *Bull. geol. Soc. Fr.,* **172**(2), 213–221.

Michon, L. & Merle, O., 2001. The evolution of the Massif Central rift: spatio-temporal distribution of the volcanism, *Bull. geol. Soc. Fr.,* **172**(2), 201–211.

Montardet, L., de Charpal, O., Roberts, D.G., Guennoc, P. & Sibuet, J.-C., 1979. Northeast Atlantic passive margins: rifting and subsidence processes, *Am. geophys. Un.,* **3**, 154–186.

Müller, B., Zoback, M.L., Fuchs, K., Mastin, L., Gregersen, S., Pavoni, N., Stephansson, O. & Ljunggren, C., 1992. Regional patterns of tectonic stress in Europe, *J. geophys. Res.,* **97**, 11 743–11 803.

Müller, B., Wehrle, V., Zeyen, H. & Fuchs, K., 1997. Short scale variations of tectonic regimes in the western European stress province north of the Alps and Pyrenees, *Tectonophysics,* **275**, 199–219.

Nehlig, P., Boivin, P., de Goër de Herve, A., Mergoil, J., Prouteau, G. & Thiéblemont, D., 2001. Les volcans du Massif central, *Géologues,*130–131, 66–91.

Nicolas, M., Santoire, J.P. & Delpech, P.Y., 1990. Intraplate seismicity: new seismotectonic data in Western Europe, *Tectonophysics,* **179**, 27–53.

Olivet, J.-L., 1996. La cinématique de la plaque Ibérique (Kinematics of the Iberian plate), *Bull. Centres Rech. Explor.–Prod. Elf Aquitaine,* **20**, 131–195

Perrier, G. & Ruegg, J.-C., 1973. Structure profonde du Massif Central francais, *Ann. Geophys.,* **29**, 435–502.

Perrot, J. *et al.*, 2005. Analysis of the Lorient earthquake (Mw = 4.3) and its aftershocks: implications in the geodynamics of the Armorican Massif, *Geophys. J. Int.,* submitted.

Reasenberg, P.A. & Oppenheimer, D., 1985. FPFIT, FPPLOT and FPPAGE: Fortran computer programs for calculating and displaying earthquake fault-plain solutions, *U.S. Geol. Surv. Open-file Rep.,* **85–739**.

Ritchie, M.E.A., Musson, R.M.W. & Woodcock, N.H., 1991. The Bishop's Castle (UK) earthquake of 2 April 1990, *TerraNova,* **2**, 290–400.

Rivera, L. & Cisternas, A., 1990. Stress tensor and fault plane solutions for a population of earthquakes, *Bull. seism. Soc. Am.,* **80**(3), 600–614.

Santoire, J.-P., 1976. Contribution à l'étude géologique du Massif du Mont Dore: la région des Couzes, *PhD thesis*, Université de Paris Sud, Orsay, p. 142.

Sobolev, S., Zeyen, H., Stoll, G., Werling, F., Altherr, R. & Fuchs, K., 1996. Upper mantle temperatures from teleseismic tomography of French Massif Central including effects of composition, mineral reactions, anharmonicity, anelasticity and partial melt, *Earth planet. Sci. Lett.,* **139**, 147–163.

Sobolev, S., Zeyen, H., Granet, M., Achauer, U., Bauer, C.F.W., Altherr, R. & Fuchs, K., 1997. Upper mantle temperatures and lithosphere-asthenosphere system beneath the French Massif Central constrained by seismic, gravity, petrologic and thermal observations, *Tectonophysics,* **275**, 143–164.

Vasseur, G., 1982. Synthèse des résultats de flux géothermique en France, *Ann. Geophys.,* **38**(2), 189–201.

Vasseur, G., Etchecopar, A. & Philip, H., 1983. Stress state inferred from multiple focal mechanisms, *Ann. Geophys.,* **1**, 291–298.

Veinante-Delhaye, A. & Santoire, J.-P., 1980. Sismicité récente de l'arc sud-armoricain et du mord-ouest du Massif Central. Mécanismes au foyer et tectonique, *Bull. geol. Soc. Fr.,* **22**, 93–102.

Zeyen, H., Novak, O., Landes, M., Prodehl, C., Driad, L. & Hirn, A., 1997. Refraction- seismic investigations of the northern Massif Central (France), *Tectonophysics,* **275**, 99–117.

Zoback, M.L., 1992. First and second order pattern of stress in the lithosphere : the world stress map project, *J. geophys. Res.,* **97**, 11 703–11 728.